The Impact of High-Frequency Sedimentation Cycles on Stratigraphic Interpretation

by

M.A. Perlmutter
Argonne National Laboratory
Argonne, Illinois 60439 U.S.A.

B.J. Radovich and M.D. Matthews
Texaco Central Exploration Division
Bellaire, Texas 77401 U.S.A.

and

C.G.St.C. Kendall
University of South Carolina
Columbia, South Carolina 29208 U.S.A.

To be published in

Predictive High Resolution Sequence Stratigraphy
Norwegian Petroleum Society

January 1997

The Impact of High-Frequency Sedimentation Cycles on Stratigraphic Interpretation

M.A. Perlmutter

Argonne National Laboratory

9700 S. Cass Ave., Argonne, IL 60439

FAX: 630-252-9281 — Email: marty_perlmutter@qmgate.anl.gov

B.J. Radovich and M.D. Matthews

Texaco Central Exploration Division

4800 Fournace Place, Bellaire, TX 77401

FAX: 713-432-2068 — Email: for Radovich: bjr@texaco.com

and for Matthews: mdm@texaco.com

C.G.St.C. Kendall

University of South Carolina

Columbia, South Carolina 29208

FAX: 803-777-6610 — Email: kendall@sc.edu

Keywords: global cyclostratigraphy, climate, stratigraphic modeling, Gulf of Mexico, Surma basin, sequence stratigraphy.

Abstract

Global cyclostratigraphy, a methodology that utilizes climate change to evaluate sediment flux, characterizes the impact of sediment cycles on stratigraphy. Climatic succession, sediment yield cycles, and the phase relationship of sediment cycles to eustatic cycles are all determined in the early stages of basin analysis. Sedimentologic information is then used to assist in sequence evaluations.

Climatic successions are intrinsically associated with global position (paleogeography) and are not necessarily synchronous with glacioeustatic sea-level cycles. A preliminary evaluation of the effect of climate on sediment supply from modern river systems indicates that sediment yield may vary by well over two orders of magnitude during one climate cycle. Consequently, basins in different climatic belts can have distinctly different volumes and lithologies for systems tracts that have similar base-level changes. The stratigraphic computer program Sedpak was utilized to examine the possible impact of different sedimentation cycles on sequence interpretation and reservoir forecasts.

The effect of sedimentation cycles on reservoir distribution in real world sequences is demonstrated with a comparison of the Miocene section of the Surma basin, Bangladesh, and the Plio-Pleistocene section of the Gulf of Mexico. In the Surma basin, reservoirs are most likely to occur in transgressive and highstand systems tracts, while reservoirs in the Gulf of Mexico are more likely in lowstand prograding complexes.

Introduction

Although the concepts of sequence stratigraphy include sediment flux as an important variable [1, 2], in practice sediment supply is commonly assumed to be predominantly a function of base-level change. Sediment supply cycles forced by paleoclimatic cycles, and the phase relationship of the sedimentation cycles with sea-level-caused base-level changes, are generally not considered. However, variations in both the volume and type of sediment delivered to a basin over a climate cycle can be significant, with the greatest changes producing a maximum volume up to two orders of magnitude greater than the minimum and a yield that may shift from conglomerate to clay. Further, because the climatic succession of a climate cycle is dependent on the (paleo)geography, the timing of maximum and minimum values of the sediment supply cycle relative to glacioeustatic sea level is dependent on location. Therefore, sediment supply cycles can affect how the distributions of potential reservoirs, seals, and source rocks are interpreted from seismic records and, therefore, affect the projection of geologic risk associated with exploration.

In this paper, we demonstrate the influence of high-frequency climate change on sediment flux and the deposition of potential reservoir rock within a stratigraphic sequence. There are three basic components in this evaluation: (1) a preliminary quantitative assessment of the effects of climate and elevation on the sediment yield of modern river systems; (2) a graphic representation of the potential differences in the time of formation of systems tracts relative to eustasy caused by shifts in the phase relationship of sediment supply and sea-level cycles, displayed by using the stratigraphic computer model Sedpak [3]; and (3) a documentation of lithologic differences in real world situations.

The concepts and applications of global cyclostratigraphy, climate change, and its effect on sediment yield and stratigraphic variability have been described previously in detail [4-8]. In summary, precession, obliquity, and eccentricity cycles with frequencies between about 20 kyr and 400 kyr periodically change the relationship between the earth and the sun, altering the annual distribution of insolation [9]. In addition, constructive and destructive interference of the primary orbital cycles produces longer-term insolation cycles in the range of 1,600 to 2,400 kyr [10]. The atmosphere accommodates these changes in insolation by varying the position and size of Hadley circulation cells, thereby shifting the global climate patterns (Figure 1) [4]. The warmest and coolest intervals are referred to as the climatic maxima and climatic minima, respectively (Figure 2). Thus, the interaction of the orbital cycles creates a repetitive spectrum of short-term climates bounded by long-term climatic maximum and minimum end-members.

As an example, the general climatic successions for the cyclostratigraphic belts in the Pleistocene/Holocene are shown in Table 1. Belts represent zones of the earth's surface, to a first approximation, which have similar climatic end-members [4]. The impacts of prevailing seasonal surface winds, oceanic temperature and circulation, and orography must be included to develop a realistic account of climatic conditions; however, by simplifying climatic succession into belts, the variable nature of the global climate pattern is easier to explain and understand. In practice, zones or belts are defined by synthesizing detailed seasonal climate maps interpreted for climatic

maximum and minimum conditions (see Table 1 map insert) [4]. Seasonal maps account for the range of paleoclimatic indicators observed for a particular geologic interval [8]. Even the simplification of climate change over an insolation cycle, as shown in Table 1, indicates a highly variable pattern when viewed globally. In general, equatorial and polar regions tend to become drier and mid-latitude regions tend to become wetter as conditions progress from the climatic maximum to minimum.

The effects of climate cycles include (1) changing sea level, produced by altering the volume of polar and alpine glaciers; (2) changing lake level, produced by varying the balance of precipitation and evaporation; (3) changing sediment production rates, mineralogy, and grain size, produced by altering weathering conditions in the sediment drainage basin; (4) changing sediment transport rates, produced by altering the hydrodynamic conditions of river systems and raising or lowering base-level; and (5) changing and shifting environments of deposition. In addition, because the timing of maximum and minimum sediment flux relative to sea and lake level is a function of climatic succession, it varies with the paleogeography of the drainage basin and is, therefore, not globally synchronous [4, 7].

Sediment supply is commonly simplified for sequence stratigraphic models and interpretations that include only those changes controlled by base-level [11-12]. High-frequency changes in sediment yield are presumably ignored in practice because it is difficult to assess their timing and magnitude [13]. As a consequence, the primary driving forces for stratigraphic variability are assumed to be nickpoint migration in the lower drainage basin, shoreline erosion and shelfal incision related to the dip-directed shift of depositional environments, and the change in accommodation space caused by the rise and fall of relative sea level.

In sequence stratigraphy, sequences are subdivided into systems tracts that represent genetically linked strata interpreted to be deposited at different phases of sea/lake level [12]. Highstand,

lowstand, transgressive, and shelf margin systems tracts are defined by the types of bounding surfaces, position within a sequence and stacking pattern, geometry, and facies associations [14]. Potential for reservoir, seal, and source rock development have been associated with systems tracts and their inherent timing with respect to sea level [12]. This approach tends to focus the seismic interpreter on the geometric changes in accommodation space, to the exclusion of sediment supply. However, by neglecting sediment supply as an important control on stratigraphy, the intrinsic variability of the lithology caused by cyclic changes in supply is overlooked. This omission can cause the actual distribution and timing of reservoir, seal, and source rock to be misinterpreted.

Climatic Succession and Sediment Flux

To ascertain changes in sediment flux caused by climate change, the quantitative effects of climate on sediment yield have to be resolved. Although a large body of evidence has demonstrated that climate is an important factor in determining yield, [15-16, 4] elevation is commonly noted as the primary control, with climate as a secondary control [17]. This generalization results from the fact that the data needed to assess the effect of climate on yield, and exactly how yield is affected by the interaction of climate and elevation, are limited.

To begin to determine the impact of elevation on load for a specific climate, we evaluated 29 modern river systems by plotting the load/unit area vs. the maximum elevation in the drainage area, using data provided by Summerfield and Hulton [18] (Figures 3 and 4). Figure 3 graphically illustrates that elevation is not the sole control on sediment load. Only 55% of the variance of these data is accounted for by elevation alone. In Figure 4, the same data are categorized by the theoretical climate at sea level in the region of the highest elevations in the drainage areas; that is, the climate of the region is estimated as if the highlands were not there. Grouping drainage basins in this manner permits evaluation of the effect of elevation on sediment flux for a single climatic regime as the climate changes from that expected at sea level. Although this analysis is preliminary and the total number of points in each category is small, significant differences in the load/unit area

are discernible once the data are subdivided by climate. Work is continuing to increase the total number of data points.

To show how sediment yield can be affected by climatic succession, estimates were made of sediment yield from provenance areas with a maximum elevation of 2 km (Figure 5). Combining the information shown in Figure 4 and Table 1, the yield from each of the idealized cyclostratigraphic belts by phase of the climate cycle (A, B1, B2, C, D1, and D2) was compared with the timing of glacioeustatic and lake-level cycles. For each belt, climatic succession is displayed vertically by phase. Sediment yield is shown by the black wavy line, with the scale at the top of the column.

On the basis of Figure 5, the greatest change in yield occurs in a climatic succession ranging from arid to subhumid, with the maximum at least two orders of magnitude larger then the minimum. This succession occurs in mid-latitude belts 3, 4a, 4b, and 5. Figure 5 also illustrates that maximum and minimum yields are not globally synchronous, because the local climatic succession is dependent on geographic location. Stated another way, sediment cycles of drainage basins in different parts of the world will not be in phase with each other. For example, in belt 1, yield is highest at the climatic maximum and lowest at the climatic minimum; in belt 4b, yield is highest at the climatic minimum and lowest in the climatic transitions, just before and after the climatic maximum. In general, belts show more than one peak episode of sediment yield over a climate cycle.

The variability of sediment flux with climatic phase becomes important when the interaction of sea level and lake level is considered (Figure 5). Conventional wisdom would suggest that as sea or lake levels fall, the associated base-level fall would increase sediment yield because of erosion of river valleys and newly exposed shoreline and shelf; during a sea- or lake-level rise, the associated base-level rise traps sediment in the fluvial drainage basins and newly flooded areas, decreasing

sediment yield to more distal regions of the depositional basin. Stratigraphic variations are commonly considered only in terms of relative sea level rather than eustasy. However, because sediment yield curves are regionally dependent and not globally synchronous, the distribution of potential hydrocarbon reservoirs may be affected by the relative timings of the sediment yield and base-level cycles.

In marine systems, the glacioeustatic curve tends to track the insolation cycle [10, 19-20] — sea level is high at the climatic maximum and low at the climatic minimum (Figure 5). Because the climatic succession of each belt relative to the insolation cycle is different, the phase relationship of yield to sea level varies. In comparison with the glacioeustatic curve, only in belts 2a, 4b, and 5 does sediment yield actually increase at some point during falling and lowstand sea level and decrease during the rise. In fact, Figure 5 demonstrates that, depending on location, maximum and minimum sediment yield can occur at any phase of eustatic sea level. The same is true for the sediment yield and lake-level curves. Coincident with volumetric changes are alterations in the conditions of weathering, affecting grain size and mineralogy, as well as the environments of deposition.

Climatic Cycles and Glacioeustasy in the Geologic Past

A brief discussion of climate and glaciation is necessary at this point to indicate that the concepts we are discussing apply to geologic periods other than the Pleistocene and Carboniferous, times for which there is hard evidence of glaciation. Although disagreement still exists in the scientific community, there is mounting evidence that glacial events may have occurred throughout the Phanerozoic, including episodes in the Cretaceous [4, 21-23]. Further, Milankovitch-frequency marine and continental stratigraphic cycles have been shown to occur in the mid-Cretaceous [22] and the mid-Eocene [24] intervals, when no glaciers are thought to have existed. This information emphasizes two very important points: (1) glacioeustatic changes (though relatively small by Pleistocene standards) may have occurred even in what are interpreted to be the warmest time in

earth's history, and (2) climate cycles and associated sedimentological cycles occurred regardless of whether there was glacial activity. Consequently, the major elements of the integration of global cyclostratigraphy with sequence stratigraphy may be applicable from at least the Cambrian.

Effects of the Phase Relationship of Sediment and Eustatic Cycles on Stratigraphy and the Projection of Reservoir Potential

The magnitude and timing of sediment yield depend on the climatic succession and the topography and size of the drainage basin. The succession, elevation, and basin size also control the grain size and mineralogy of the sediments being delivered from a specific parent rock and the types of settings in which sediments are deposited.

To demonstrate the potential effects of climate and sediment cycling on stratigraphy, four idealized phase relationships between sediment yield and eustatic sea/lake level were simulated by using the stratigraphic computer model Sedpak. Sedpak is a parametric model that simulates the two-dimensional sedimentologic/stratigraphic geometry of a basin by integrating variables related to tectonic subsidence and uplift, eustasy, and sedimentation [3]. In the experiment, only the phase relationships between sediment supply and sea-level cycles were varied; all other inputs were kept the same. The phase relationships that were evaluated were (1) sedimentation rates maximum during the eustatic fall, minimum during the rise (Figures 6 and 7); (2) sedimentation rates maximum at eustatic lowstands, minimum at highstands (Figures 8 and 9); (3) sedimentation rates maximum during the eustatic rise, minimum during the fall (Figures 10 and 11); and (4) sedimentation rates maximum at eustatic highstands, minimum at lowstands (Figures 12 and 13). In these simulations, a simple sinusoid was assumed to represent both the changes in the sediment supply and eustatic sea level. Maximum sediment supply was designated as five times the minimum supply, and the sand/shale ratio was equal to one-third at all times. The amplitude of the sea-level cycle was 40 m. Shelf erosion during falling and low sea level was prescribed to be 10%. The duration of the simulation was 500 kyr. In the figures, black lines indicate time steps and black dots indicate coastline position. This version of Sedpak does not inherently simulate

detached lowstand deposits. These experiments are a more rigorous examination of the interaction of sedimentation and eustasy reported previously [13, 25-27].

In these experiments, tectonic subsidence plays a minor role in forcing base-level change. Subsidence was simulated as hinged and nonvarying through time at any one position, with rates increasing with distance from 0 cm/kyr at 0 km to 3 cm/kyr at 1,750 km (not shown on the figure); these rates are low compared to the rates of change of eustasy and sediment supply. The simulations, therefore, display the possible impact of a varying sediment supply on the shift of base-level forced by eustasy and show how the interpretation of the timing of systems tracts is related to eustasy and sediment supply.

Cross sections indicating the water depth at the time of deposition (Figures 6, 8, 10, and 12) and partitioning of deposition by high and low eustatic sea level (Figures 7, 9, 11, and 13) were made for each phase relationship. Depth sections were used to evaluate the general distribution of depositional settings through time, the relative amount of progradation and aggradation, and the shifts in stacking geometry. Sequence boundaries (SB), transgressive surfaces (TS), and maximum flooding surfaces (MFS) were interpreted from the depth cross section. Interpreted surfaces from the depth section were replotted on the cross section displaying strata as deposited during high and low stages of eustasy. In this manner, the timing of specific surfaces and systems tracts could be compared with eustatic sea-level change. The results are summarized in Table 2.

The timing of occurrence of the major stratal surfaces was interpreted in the manner of Vail et al. [28]. The maximum flooding surface, corresponding to the time at which base-level had its most landward position and commonly associated with the occurrence of a condensed section [2], was read directly from the simulation output. The maximum flooding surface matches the time when Sedpak calculates shoreline position, displayed as a black dot, to be most landward (see Figures 6-13). Sequence boundaries, indicated by downward and basinward shifts of coastal onlap and

facies, were interpreted in the simulations to occur at the time of rapid downward shift of coastal onlap, as indicated by a shift in shoreline position and depth facies. The transgressive surface, indicative of the landward shift in base-level, was picked at the onset of backstepping onlap. Lowstand prograding complexes, commonly associated with the early rise of base-level, were presumed to occur below the transgressive surface. We recognize that there are other schools of thought on how sequences and surfaces are picked. However, our interpretations were made consistently, using the criteria described above. Therefore, any shifts in the relative timing of surfaces caused by the interaction of sediment supply and eustasy will occur regardless of the methodology that is used to define them.

When sediment supply is highest at the inflection point during the eustatic fall and lowest at the inflection point of the rise (Figure 6), a thick prograding geometry occurs in the lowstand wedge, followed by a thin, transgressive aggradational unit. For this system, the sequence boundary occurs during the mid-fall, just prior to the inflection point; the transgressive surface, in the early stages of the rise, just after lowstand; and the maximum flooding surface, during the late rise, just prior to highstand (Figure 7; Table 2). The condensed section occurs coincident with the lowest sedimentation rates, during the eustatic rise, and the lowstand prograding complex, representative of the early rise of base-level, is deposited very late in the fall of eustasy and at the low (Table 2). In this experiment, where coarse material is always one-third of the total yield, the highest volume of coarse material is concurrent with the highest yield. Therefore, the highest potential for reservoir deposition would occur prior to the lowstand prograding complex in basin floor and slope fans (not modeled by Sedpak).

When sediment supply is highest during the eustatic low and lowest during the high (Figure 8), a thin prograding geometry occurs in the lowstand wedge, followed by a thick, transgressive aggradational unit. For this system, the sequence boundary occurs at the very early stages of eustatic fall, just after highstand; the transgressive surface, in the early stages of the rise; and the maximum flooding surface, at highstand (Figure 9; Table 2). The condensed section occurs

coincident with the lowest sedimentation rates, during the eustatic high, and the lowstand prograding complex is deposited during the low to early rise of eustasy (Table 1). In this experiment, the highest potential for reservoir deposition occurs during the later stages of deposition of submarine fans and during the early stages of deposition of the lowstand prograding complex.

When sediment supply is highest at the inflection point of the eustatic rise and lowest at the inflection point of the fall (Figure 10), only a very thin prograding geometry occurs in the lowstand wedge, followed by thick, aggradational transgressive and highstand units. For this system, the sequence boundary occurs at the eustatic low; the transgressive surface, in the mid-rise at the inflection point; and the maximum flooding surface, in the very late rise, just prior to highstand (Figure 11; Table 2). The condensed section occurs coincident with the lowest sedimentation rates, during the eustatic fall, and the lowstand prograding complex is deposited during the mid-rise of eustasy (Table 2). In this experiment, the highest potential for reservoir deposition occurs during the later stages of the deposition of the lowstand prograding wedge and in the transgressive systems tract.

When sediment supply is highest during the eustatic high and lowest during the low (Figure 12), the lowstand wedge is very thin. The lowstand wedge is followed by a thick, transgressive aggradational unit and highstand deposits with more prograding geometries than with highest sediment yield during the rise. The lack of sediment in the lowstand position creates resolution problems, making some of the surface picks difficult. For this system, the sequence boundary occurs in the early fall of eustasy, midway between highstand and the inflection point; the transgressive surface, at the low; and the maximum flooding surface, in the late rise, midway between the inflection point and highstand (Figure 13; Table 2). The condensed section occurs coincident with the lowest sedimentation rates, during the eustatic low; the lowstand prograding complex is deposited during the late fall of eustasy (Table 2). In this experiment, the highest

potential for reservoir deposition occurs during the later stages of the deposition of the transgressive systems tract and during the deposition of the highstand systems tract.

These experiments were simplified to permit relatively straightforward descriptions and interpretations by using single sinusoids with relatively low-amplitude yield cycles. Even under these conditions, results demonstrated that significant variation occurred in the timing of surfaces and systems tracts relative to the eustatic cycle. Real world climatic successions can, of course, produce a more variable yield cycle with larger amplitudes and multiple peaks, causing a more complex interaction of yield and eustasy than has been modeled here. Therefore, in order to forecast the distribution of the lithofacies with the highest probability of containing reservoir, it is important to understand the climatic succession and the phase relationship of the yield and eustatic cycles at the highest frequency of climate change.

Although not part of these particular experiments, the sand/shale ratio can change significantly during a climate cycle as a result of the variation in weathering [4]. In fact, for certain climatic successions, sand percentages can increase as total volume decreases. Thus, for some regions, the timing of optimal reservoir potential will also be a function of the balance between the total volume of coarse material and the coarse fraction of the total volume of sediment.

Real World Examples: Surma Basin, Bangladesh, and Gulf of Mexico.

To demonstrate that the occurrence of reservoirs can be controlled by climatic succession, we compared the predicted and interpreted distribution and timing of reservoirs and potential reservoirs (sand beds) in the late Miocene section of the Surma basin, Bangladesh (Figures 14-16), and a Plio-Pleistocene section of the Gulf of Mexico in the area of the Mississippi River (Figures 17-19). Climate interpretations and associated sedimentation and reservoir forecasts were made at the scale of precession.

Surma Basin: In the late Miocene, conditions during the climatic maximum in the fluvial drainage area of the Surma basin were interpreted to be tropical wet, with a short dry season. Sediment yield was very fine-grained as a result of vigorous biochemical weathering. As the conditions cooled toward the climatic minimum, a wet summer, dry winter monsoon developed, increasing the volume and coarseness of sediment yield. Alpine glaciers may have formed at the climatic minimum in the higher elevations of the headlands, with seasonal melting adding to the overall load. As the climate continued to warm, the area became wetter and the volume and coarseness of the yield fell.

To determine the phase relationship of the sediment yield and eustatic cycles, we must consider that at the scale of precession (20 kyr), the northern and southern hemisphere are 180° out of phase; a climatic maximum in the northern hemisphere corresponds to a climatic minimum in the southern hemisphere. In the late Miocene, only the southern hemisphere had a large polar icecap, and therefore the southern hemisphere controlled glacioeustasy. As a result, the time of the highest volume and coarsest sediment yield to the Surma basin (northern hemisphere climatic minimum) corresponded to high eustatic sea level (southern hemisphere climatic maximum, glacial minimum). The time of the lowest volume, finest-grained yield (northern hemisphere climatic maximum) corresponded to low sea level (southern hemisphere climatic minimum, glacial maximum). Sediment yield would have been highest in and around high sea level, possibly peaking just as sea level began to fall as the alpine glaciers melted. Total yield and grain size would then have decreased as tropical wet conditions developed in the drainage basin toward low sea level. However, continued high levels of river discharge would have caused erosion of the shelf as base-level fell. Based on the timing of the sediment yield cycle relative to the eustatic cycle, the potential for major reservoir-forming strata should be highest in later transgressive and highstand positions.

In comparison with the idealized stratigraphic models described previously, the Surma basin is expected to be a modification of the simulation displaying the effects of maximum yield around the

eustatic high (Figures 12 and 13; Table 2). Modifications should be related to the decrease in grain size that occurred as the system became more humid, and to the possible flush of coarse sediment associated with the melting of alpine glaciers during the early fall of glacioeustasy. In this scenario, the transgressive surface should occur immediately at the onset of the eustatic rise, and the lowstand prograding complex should have been deposited late in the eustatic fall, during the time of fine-grained sediment yield. The transgressive systems tract would then include all sediments deposited during rising eustasy. On the basis of the correlation of yield with sea level, the potential for deposition of reservoir-forming strata should increase toward the eustatic high, with the highest reservoir potential in the later transgressive and highstand system tracts. A sediment pulse early in the sea-level fall would have increased this potential and increased the rate of highstand progradation.

Radovich et al. [29] summarized the strata in the Surma basin as cyclic, with sandy, shallow shelf transgressive and highstand systems tracts; muddy, silty, marginal marine lowstand wedges; and prograding complexes (Figures 14-16). Thin, muddy condensed sections overlie transgressive shoreline sands. These observations and interpretations match the forecasts made using global cyclostratigraphy.

Gulf of Mexico: The relationship of the sediment yield cycle of the Mississippi River drainage basin to the glacioeustatic cycle in the late Pliocene and the Pleistocene was previously evaluated by Perlmutter [30] and Kolla and Perlmutter [13]. In summary, the maximum yield was estimated to be up to 13 times the minimum yield and was projected to have occurred during the early to mid-rise of eustasy. The maximum coarse yield, up to 20 times the minimum coarse yield, was also forecast to occur at this time. Minimum total and coarse yields occurred in association with the lower runoff produced by cold temperatures and maximum glaciation during the eustatic low (Figure 17). Weathering and transport conditions at the climatic maximum caused the Mississippi drainage basin to deliver more fine-grained sediments in association with highstand.

In accordance with this information, the potential for major reservoirs should be highest in strata deposited during the early to mid-rise of eustasy, presumably in well-developed lowstand prograding complexes and possibly in early transgressive systems tracts. In Gulf regions directly associated with the Mississippi Canyon, Kolla and Perlmutter [13] have suggested that the extremely high sediment loads associated with the deglaciation kept the Mississippi River mouth connected to the canyon head until at least the mid-rise. This situation also permitted the continued formation of thick, sandy fans well into the mid-rise, concurrent with the deposition of the thick, sandy, lowstand prograding complexes that formed in non-canyon areas.

In comparison with the idealized stratigraphic models described previously, the late Pliocene to Pleistocene stratigraphy of the Gulf should be evaluated as a combination of two simulations: maximum yield during the early to mid-eustatic rise (slightly earlier than the simulation) and minimum yield at the low. On the assumption that the variations with respect to eustasy of the interpretations of key surfaces and strata from these simulations are applicable to real world situations (referring to Figures 10-13 and Table 2), the shift in stratal geometry interpreted as the transgressive surface was delayed relative to eustatic rise, expanding the time of deposition of lowstand prograding complexes and placing them well into the rapid eustatic rise.

Prior to the glaciation of North America in the late Pliocene (~2.5 - 3 ma) [31], climate conditions in the western headlands of the Mississippi drainage basin, where most of the sediment was produced, were warm temperate/subhumid to dry during the climatic maximum and cool temperate/humid to subhumid at the climatic minimum [4, 7]. Alpine glaciers may have formed in the higher elevations of headlands during the climatic minimum. These climates were used to estimate early Pliocene sediment yield by means of Figure 4; yield was highest during the climatic maximum (~9,000 kg/km^2/yr) and lowest during the climatic minimum (~3,000 kg/km^2/yr). Seasonal melt from alpine glaciers during the climatic minimum worked to counterbalance the effect of the reduced amount of water in the hydrologic cycle due to lower temperatures. These

estimates suggest that maximum yield was two to three times minimum yield. The shift to a cooler but more humid climate in the western portion of the drainage basin would have tended to reduce grain size.

In the early Pliocene, only the southern hemisphere had a large polar icecap and, therefore, the southern hemisphere controlled glacioeustasy. As a result, high eustatic sea level (southern hemisphere climatic maximum, glacial minimum) corresponded to the time of the lowest volume yield (northern hemisphere climatic minimum). As sea level fell, the climate in the Mississippi drainage basin warmed, runoff increased, and alpine glaciers melted, increasing the sediment load. The associated fall in base-level, combined with an active river system, allowed erosion of the shelf, conceivably making the total volume of sediment delivered to the Gulf of Mexico during the fall coequal to that of low eustatic sea level, the time of the northern hemisphere climatic maximum and highest yield from the Mississippi drainage basin. As sea level rose, the climate in the drainage area became cooler and more humid, decreasing yield and grain size. The addition of accommodation space caused by rising eustasy would have significantly reduced the volume of sediment reaching the Gulf. The resulting yield cycle is skewed toward mid-fall and low eustasy, in comparison to the late Pliocene-Pleistocene section in which maximum supply and coarse yield occurred during the early to mid-rise of eustasy.

In comparison with the idealized stratigraphic models described previously, the early Pliocene stratigraphy should be evaluated with the simulation showing the effects of maximum yield occurring during eustatic sea-level fall and minimum yield during the rise, with a modification that stretches peak yield through lowstand (Figures 6-9). If applicable to real world situations (referring to Figures 6-9 and Table 2), the shift in stratal geometry interpreted as the transgressive surface began early in the eustatic rise, ending the interval of deposition of lowstand prograding complexes earlier in the eustatic cycle than those deposited in the late Pliocene-Pleistocene section. Nevertheless, the highest potential for sandy reservoirs in the Gulf of Mexico should be in systems

tracts deposited in relative lowstand position, fans and prograding complexes. This is in direct contrast to the sandy reservoirs in the Surma basin, which occur in more updip positions, in transgressive and highstand systems tracts.

A detailed sequence stratigraphic analysis of a regional line on the Louisiana shelf, Gulf of Mexico, was made by Radovich et al. [32, 26] (Figures 18 and 19). These authors integrated seismic interpretation, electric logs, and biostratigraphy to interpret systems tracts in five prograding sequences ranging in age from early Pliocene to early Pleistocene. Biostratigraphy indicated that water depths in the area of study were predominantly outer shelf and slope during deposition of transgressive and highstand systems tracts. This location permitted excellent definition of lowstand prograding complexes, which were expanded and sand-rich compared to the transgressive and highstand systems tracts, which are mostly thin and predominantly shaly. Thus, the interpretation of the distribution of potential reservoir-forming sands made using sequence stratigraphy again coincides with the forecasts made using global cyclostratigraphy.

Summary and Discussion

Climatic succession is interpretable and mappable and is a function of global position. Preliminary investigations indicate that climatic succession may cause sediment flux to vary by over two orders of magnitude during the span of one insolation cycle. Because succession is a function of location, and glacioeustatic sea level tends to track the insolation cycle, the phase relationship of the sediment yield cycle to glacioeustasy varies as a function of paleogeography and is, therefore, not necessarily related to any specific stage of sea-level change.

Simplified simulations using the computer model Sedpak were used to demonstrate the phase relationships between sediment cycles and base-level changes produced by eustatic and lake cycles. For each simulation, cross sections were made indicating the environments of deposition tied to water depth and the distribution of strata relative to high and low eustasy. Sequence boundaries,

transgressive surfaces, maximum flooding surfaces, and condensed sections interpreted from shifts in stacking geometry on the depth section were replotted on the cross section, displaying strata as deposited during high and low stages of eustasy. In this way, interpreted relative base-level change and the timing of deposition of systems tracts could be compared with eustatic sea-level change.

The modeling suggested that the timing of the sediment supply cycle with respect to eustatic sea level affects the lithologies and depositional systems related to base-level changes. In three of the four simulations, phase lags caused the sequence boundary to be interpreted to have occurred between the early and mid-fall of eustasy (Table 2). In the fourth simulation, with low yield during the fall and high yield during the rise, the sequence boundary was interpreted to have occurred at lowstand. Low resolution of time lines as a consequence of low sedimentation rates during the fall made the analysis of this particular simulation difficult. The interpretation of the transgressive surface varied from lowstand to the mid-rise, placing the lowstand prograding complexes between the late fall and mid-rise of eustasy, depending on the sediment yield. This interpretation has interesting consequences in terms of the likely lithofacies and reservoir potential for each of these systems tracts. For example, if one makes the simplifying assumption that maximum reservoir potential occurs during maximum yield, then the lowstand prograding complex with the highest reservoir potential would be the one associated with maximum supply during the rise. Sands should be expected throughout this interval. The lowstand prograding complex with the lowest reservoir potential would be the one associated with maximum supply at highstand. This prograding complex would have formed well past peak supply, and potential would decrease upward in the interval. Maximum supply at lowstands produces a prograding complex with high initial potential, decreasing upward in the interval as sedimentation waned. Maximum supply during the fall produces a prograding complex with moderate potential, which again would decrease upward in the interval as sedimentation waned.

The distribution of reservoirs in the Gulf of Mexico Pleistocene section in the area of the Mississippi River was compared with the late Miocene section of the Surma basin, Bangladesh, to demonstrate the effect climatic succession has on lithostratigraphy. In these cases, actual distributions closely matched the distribution forecasts obtained by using global cyclostratigraphic methods. Potential reservoirs in the Gulf were associated with thick, sandy, lowstand prograding complexes, while reservoirs in the Surma basin were associated with transgressive and highstand systems tracts.

Even in the relatively uncomplicated simulations considered here, variation occurred in the timings of surfaces and systems tracts relative to the timing of the eustatic cycle. As demonstrated, sediment yield cycles in real world situations are more complex, with larger amplitudes and multiple peaks, causing more complex stratigraphy than in these models. However, integrating climate allowed the sediment yield cycle and its phase relationship to the eustatic cycle to be understood a priori, thereby making lithologic variability more predictable and reducing the risk associated with forecasting reservoirs.

Acknowledgments

We gratefully acknowledge Texaco, Inc., for permission to publish this paper. Sedpak was developed by C. St. C. Kendall and his associates at the University of South Carolina. This work is supported by the U.S. Department of Energy, Assistant Secretary for Energy Efficiency and Renewable Energy, under Contract W-31-109-Eng-38. We want to thank M. Gading for an insightful review and F. Bennett for diligent editing.

References

1. Posamentier HW, Vail PR. Eustatic controls on clastic deposition II — sequence and systems tract models. In: Sea-level changes — an integrated approach. Soc. Econ. Paleont. Min. Spec. Pub. 1988; 42:125-154.

2. Posamentier HW, Jervey MT, Vail PR. Eustatic controls on clastic deposition I — conceptual framework. In: Sea-level changes — an integrated approach. Soc. Econ. Paleont. Min. Spec. Pub. 1988; 42:109-124.

3. Kendall CGStC, Moore P, Strobel J, Cannon R, Perlmutter M, Bezdek J, Biswas G. Simulation of the sedimentary fill of basins. In: E.K. Franseen, W.L. Watney, C.G.St.C. Kendall, and W. Ross (eds.), Sedimentary Modeling, Kansas Geol. Survey Bull. 1991; 233:9-30.

4. Perlmutter MA, Matthews MD. Global cyclostratigraphy: a model. In: T. Cross (ed.), Quantitative dynamic stratigraphy. New Jersey: Prentice Hall, 1989; 233-260.

5. Perlmutter MA, Matthews MD. Global cyclostratigraphy. In: W.A. Nierenberg (ed.), Encyclopedia of earth systems science. Academic Press, 1992; 379-393.

6. Perlmutter MA, Matthews MD. Global cyclostratigraphy: predicting stratigraphic response to Milankovitch Cycle. In: C.B. Cecil and N.T. Edgar (eds.), Predictive stratigraphic analysis — concept and applications. U.S.G.S. Survey Bull., 1994; 2110:6-7.

7. Matthews MD, Perlmutter MA. Global cyclostratigraphic analysis of the Green River basin. In: P.L. de Boer, D.G. Smith (eds.), Orbital forcing and cyclic sequences. Int. Assoc. Sed. Spec. Pub. 1994; 19:459-481.

8. Perlmutter MA, Brennan PA, Hook SC, Dempster K, and Pasta D. Global cyclostratigraphic analysis of the Seychelles Southern Shelf for potential reservoir, seal, and source rocks. In: T.A. Davis and M. Coffin (eds.), Paleoceanography and environments of exploration of the Indian Ocean basin and margins. Sed. Geol. Spec. Iss. 1995; 96/1-2:93-118.

9. Milankovitch MM. Canon of insolation and the ice age problem. Transactions of the Royal Serbian Academy, Beograd (former Yugoslavia), 1941. English translation by Israel Program for Scientific Translation, published for the U.S. Dept. of Commerce and the National Science Foundation.

10. Matthews RK, Frohlich C. Orbital forcing of low frequency glacioeustasy. J. Geophys. Res. 1991; 96 B4:6797-6803.

11. Weimer RJ. Developments in sequence stratigraphy. Amer. Assoc. Petrol. Geol. Bull. 1992; 76/7:965-982.

12. Mitchum RM, Van Wagoner JC. High frequency sequences and their stacking patterns: sequence-stratigraphic evidence of high frequency eustatic cycles. Sed. Geol. 1991; 70/2-4:131-160.

13. Kolla V, Perlmutter MA. Timing of turbidite sedimentation — Mississippi fan. Amer. Assoc. Petrol. Geol. Bull. 1993; 77/7:1129-1141.

14. Van Wagoner JC, Mitchum RM, Sarg JF, Loutt TS, Hardenbol J, Posamentier HW, Vail PR. An overview of the fundamentals of sequence stratigraphy and key definitions. In: Sea level changes: an integrated approach. Soc. Econ. Paleont. Min. Spec. Pub. 1988; 42:39-45.

15. Garner HF. Stratigraphic-sedimentary significance of contemporary climate and relief in four regions of the Andes Mountains. Geol. Soc. Amer. Bull. 1959; 70:1327-1368.

16. Schumm SA. The fluvial system. New York: Wiley, 1977; 338 p.

17. Milliman JD, Syvitski JPM. Geomorphic/tectonic control of sediment discharge to the ocean: the importance of small mountainous rivers. J. Geol. 1992; 100:525-544.

18. Summerfield MA, Hulton NJ. Natural controls of fluvial denudation rates in major world drainage basins. J. Geophys. Res. 1994; 99 (B7):13,871-13,883.

19. Kukla G, Gavin J. Insolation regime of the warm to cold transitions. In: G.J. Kukla and E. Went (eds.), NATO ASI Series 1992; Vol. 13:307-339.

20. Berger AL. Astronomical theory of paleoclimates and the last glacial-interglacial cycle. Quaternary Science Reviews 1992; 11:571-581.

21. Frakes LA, Francis JE. A guide to Phanerozoic cold polar climates from high-latitude ice rafting in the Cretaceous. Nature 1988; 333: 547-549.

22. Kemper E. Das Klima der Kreide-Zeit. Geol. Jb. 1987; A 96:5-185.

23. Kerr RA. Ancient sea level swings confirmed. Science 1996; 272:1097-1098.

24. Bradley WH. The varves and climate of the Green River Epoch. U.S.G.S. Prof. Pap. 1929; 154:86-110.

25. Perlmutter MA, Matthews MD. Global cyclostratigraphy: effects of timing of sediment delivery to continental margins relative to sea level. AGU Chapman Conference on Long-Term Sea Level Changes, Snow Bird, UT, April 1989.

26. Perlmutter MA, Matthews MD. Global cyclostratigraphy, sediment flux, and continental margin stratigraphy. AAPG Ann. Mtg., Calgary, Alberta, Canada, June 1992.

27. Kendall C.G.St.C, Whittle GL, Ehrlich R, Moore PD, Cannon RL, Hellmann DR. Computer sedimentary simulation models sequence stratigraphy. Oil and Gas Journal 1993; 91/17:46-51.

28. Vail PR, Audemard F, Bowman SA, Eisner PN, Preez-Cruz G. The stratigraphic signatures of tectonics, eustasy, and sedimentation — an overview. In: G. Einsele, W. Ricken, and A. Seilacher (eds.), Cycles and events in stratigraphy, Heidelberg: Springer Verlag, 1991; 617-659.

29. Radovich BJ, Hoffman MW, Perlmutter MA. Upside-down sequence stratigraphy, sandy highstands, and muddy prograding complexes in the Surma basin, Bangladesh. Amer. Assoc. Petrol. Geol. Ann. Mtg. Program, Houston, Texas, March 1995, p. 79A.

30. Perlmutter MA. Deep water clastic reservoirs in the Gulf of Mexico: a depositional model. Geo-Marine Letters 1985; 5:105-112.

31. Galloway WE, Bebout DG, Fisher WL, Dunlap JB Jr, Cabrera-Castro R, Lugo-Rivera JE, Scott TM. Cenozoic. In: A. Salvador (Editor), The Gulf of Mexico Basin, The Geology of North America, 1991;Vol. J: Geol. Soc. Amer. Inc., Boulder, Colo., 245-324.

32. Radovich BJ, Powell T, Lovell M, Mitchum RM. Sequence stratigraphy interpretation of the central shelf area, offshore Louisiana. Gulf Coast Section Soc. Econ. Paleont. and Mineral. Eleventh Annual Research Conference Program and Abstracts, Dec. 2, 1990; 287-298.

Figure Captions:

Figure 1. Atmospheric response to climate change. The general Hadley circulation pattern of the atmosphere migrates with changes in insolation. Note that the general distribution of humidity also shifts as a function of cell size and position [7].

Figure 2. Climatic maxima and minima. The interference of Milankovitch cycles causes seasonal insolation to vary. The warmest periods are referred to as maxima, phase A; the coolest as minima, phase C; the cooling transition as phase B; and the warming transition as phase D. Interference patterns produce intervals with warmer or more persistent maxima and cooler or more persistent minima.

Figure 3. Sediment yield/unit area vs. elevation (data from [18]).

Figure 4. Sediment yield/unit area vs. elevation subdivided by climate. Numbers refer to rivers: (1a) Brahamaputra, (1b) Ganges, (2) Amazon, (3) Mississippi, (4) Chiang Jiang, (5) Indus, (6) Mekong, (7) Colorado, (8) Orinoco, (9) MacKenzie, (10) Huang He, (11) Nile, (12) La Plata, (13) Yukon, (14) Danube, (15) Orange, (16) Amur, (17) Zaire, (18) Shatt-El-Arab, (19) Zambezi, (20) Niger, (21) Murray, (22) Columbia, (23) Rio Grande, (24) Ob, (25) Lena, (26) Yenisei, (27) Sao Francisco, and (28) Kolyma. Estimates of yield for headlands with a climatic range were made by averaging values.

Figure 5. Sediment yield for each cyclostratigraphic belt by climate phase, sea level, and lake level. Solid curves are sediment yield and dashed curves are lake level; sea level is shown on the right. Estimates from data are indicated with asterisks. Abbreviations are as follows: Tr = tropical; Te = temperate; P = polar; VH = very humid; H = humid; SH - subhumid; D = dry; A = arid. See text for explanation.

Figure 6. Stratigraphic simulation by using Sedpak. Depth cross section shows the result of maximum sediment input during sea-level fall and minimum during sea-level rise. Each color represents a depositional depth range. Maximum depth of that environment is indicated in the legend. Black dots denote position of the ultimate coastline for each time step. Fluvial sediments are deposited above sea level. Eustatic sea level and sediment supply curves are shown on the right-hand side of the figure. Yellow represents the sand component (33%) and green the shale component (67%).

Figure 7. Cross section displaying deposition during high and low eustatic sea level by using Sedpak. This plot differentiates by color the strata deposited at high sea level from strata deposited at low sea level. Colors are keyed to the sea-level curve at the right. Sequence boundaries (SB), transgressive surfaces (TS), and maximum flooding surfaces (MFS) interpreted from Figure 6 are replotted here to compare their timing with eustatic sea-level change.

Figure 8. Stratigraphic simulation by using Sedpak. Depth cross section shows maximum sediment input at lowstand and minimum input at highstand. See Figure 6 for general description.

Figure 9. Cross section displaying deposition during high and low eustatic sea levels by using Sedpak. Stratigraphic surfaces interpreted from Figure 8 are displayed to indicate their timing relative to eustasy. See Figure 7 for general description.

Figure 10. Stratigraphic simulation by using Sedpak. Depth cross section shows maximum sediment input during rising sea level and minimum input during falling sea level. See Figure 6 for general description.

Figure 11. Cross section displaying deposition during high and low eustatic sea levels by using Sedpak. Stratigraphic surfaces interpreted from Figure 10 are displayed to indicate their timing relative to eustasy. See Figure 7 for general description.

Figure 12. Stratigraphic simulation by using Sedpak. Depth cross section shows maximum sediment input at highstand and minimum input at lowstand. See Figure 6 for general description.

Figure 13. Cross section displaying deposition during high and low eustatic sea levels by using Sedpak. Stratigraphic surfaces interpreted from Figure 12 are displayed to indicate their timing relative to eustasy. See Figure 7 for general description.

Figure. 14. Surma basin location map for interpreted cross sections [26].

Figure 15. Interpreted seismic section from the Surma basin [26]; see Figure 14 for location. Lowstand prograding complexes (lavender) are mud-prone. Highstand (orange) and transgressive (green) systems tracts are sandy-prone. The lime green, bright orange, and blue circles are also noted in Figure 16 for reference.

Figure 16. Sequence stratigraphic cross section from the Surma basin [26] (see Figure 14 for location). Lime green, bright orange, and blue circles are also noted in Figure 15.

Figure 17. Potential sediment transport (P.T.) via the Mississippi River vs. shelfal accommodation (A.S.) space [13, 27]. Calculations indicate that the largest sediment yield occurred during rapidly rising sea level, with the smallest yield at the low. The curve of accommodation space on the shelf tracks sea level, indicating that the volume of sediment transported by the Mississippi River during maximum yield was more than enough to overwhelm all available shelfal space until late in the rise.

Figure 18. Gulf of Mexico location map for interpreted cross section X-X' [29].

Figure 19. Correlated log cross section X-X'. Vertical exaggeration is 6. SP curves indicate fining (right slant) or coarsening (left slant) upwards. Lowstand prograding complexes (PGC; shaded) are sand-prone [29]. Highstand (HST) and transgressive (TST) systems tracts are mud-prone.

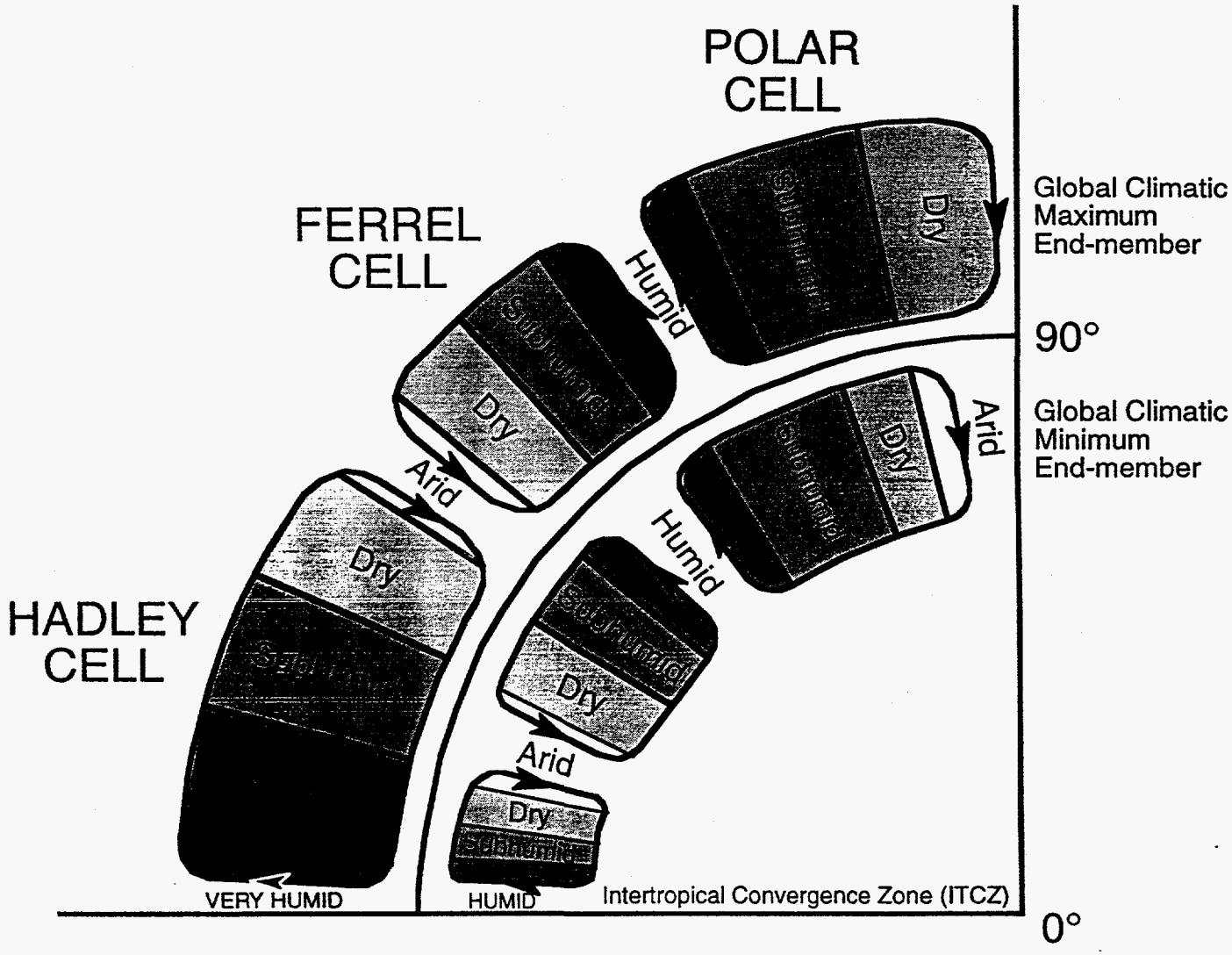
POLAR CELL
FERREL CELL
HADLEY CELL
Global Climatic Maximum End-member
90°
Global Climatic Minimum End-member
Humid
Arid
Dry
Arid
Humid
Dry
Arid
Dry
VERY HUMID
HUMID
Intertropical Convergence Zone (ITCZ)
0°

Fig 1

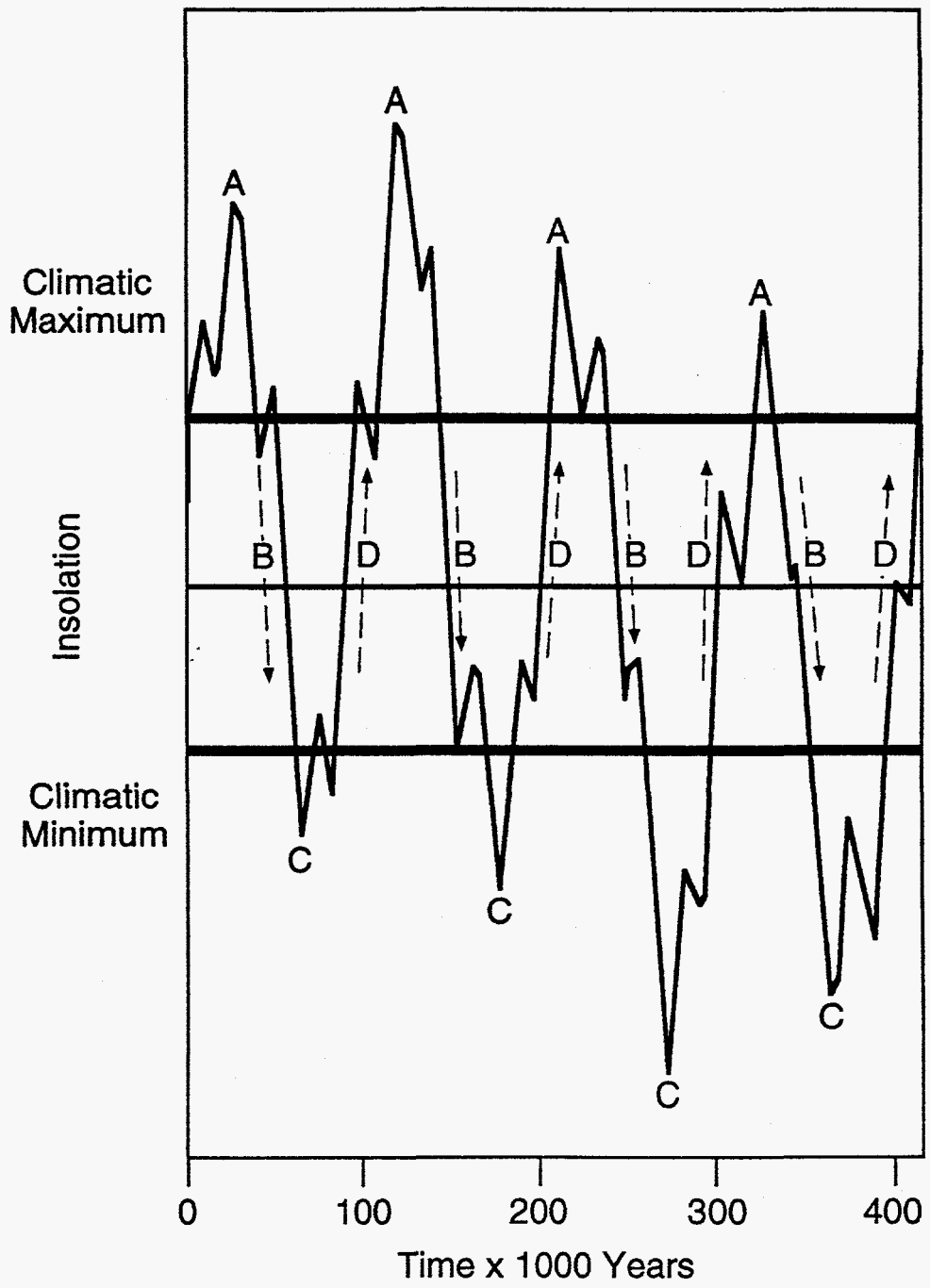
Climatic Maximum
Insolation
Climatic Minimum
A
A
A
A
B
D
B
D
B
D
B
D
C
C
C
C
0
100
200
300
400
Time x 1000 Years

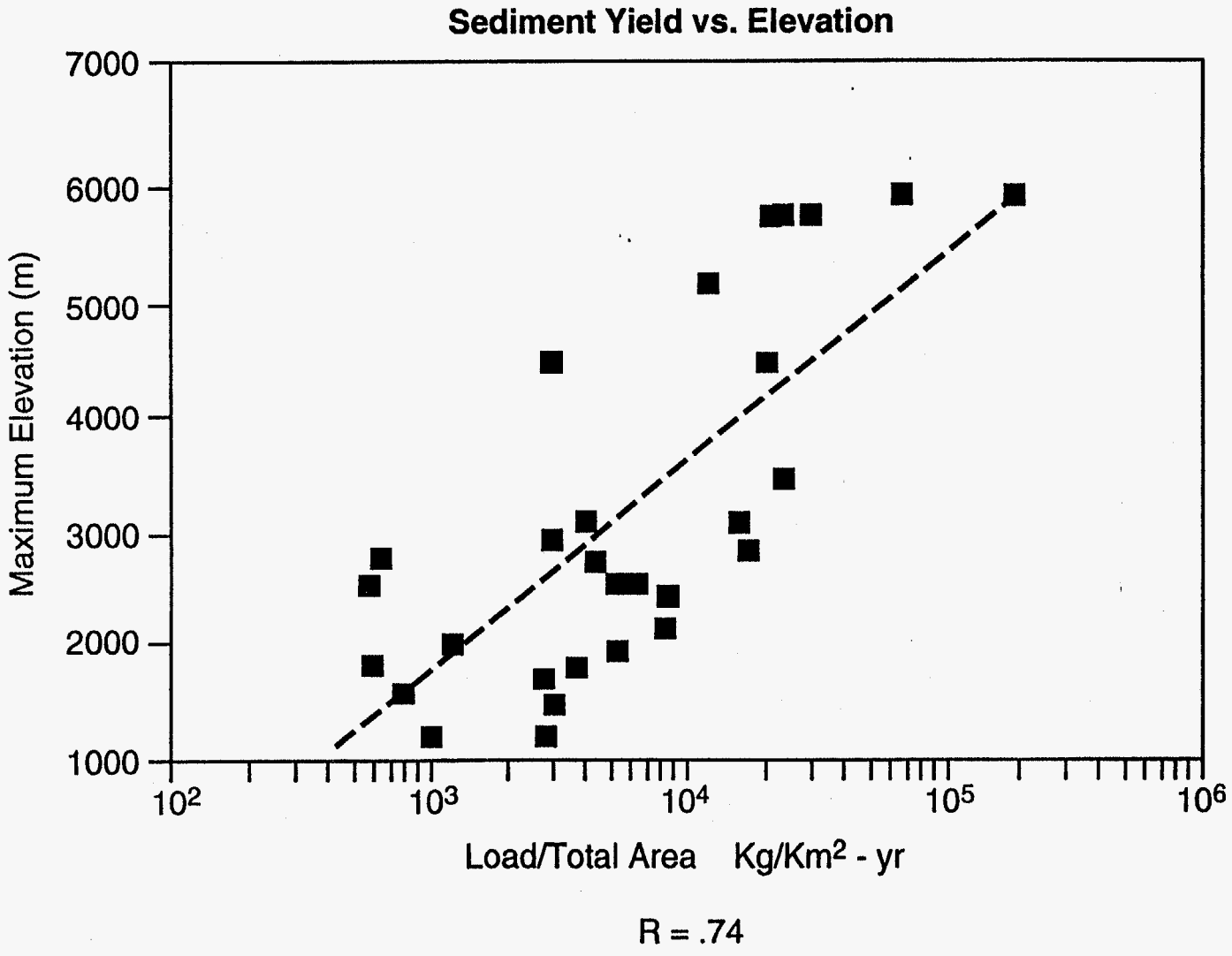
Sediment Yield vs. Elevation
7000
6000
5000
4000
3000
2000
1000
Maximum Elevation (m)
10^2
10^3
10^4
10^5
10^6
Load/Total Area Kg/Km^2 - yr
R = .74

Fig 3

Sediment Yield vs. Elevation as a Function of Climate

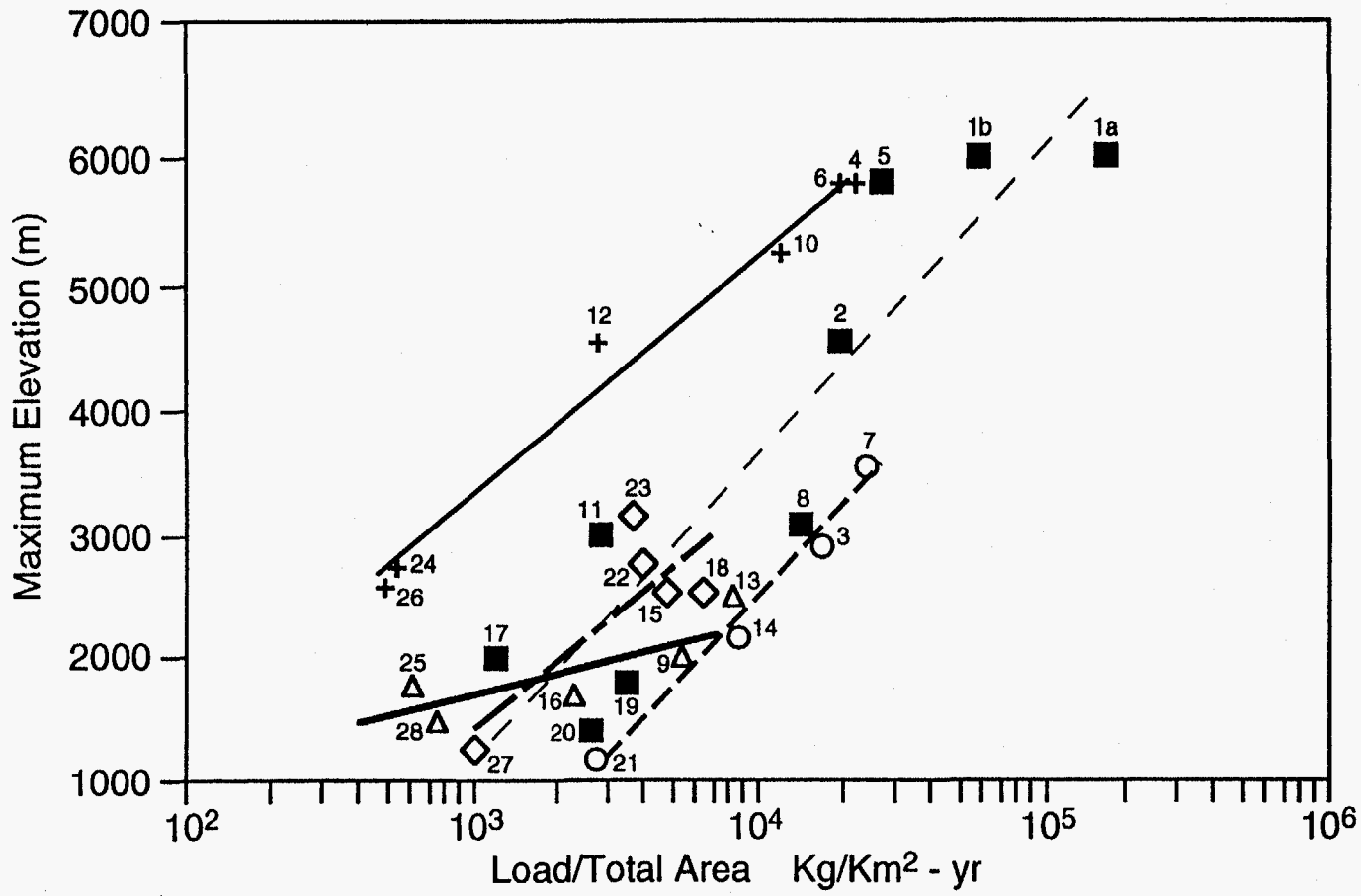

■ Tropical/Monsoon	R = .91	Δ Polar	R = .79
○ Temperate/SubHumid	R = .99	+ Temperate/Humid	R = .99
◇ Temperate/Dry	R = .88	All Points	R = .74

Fig. 4

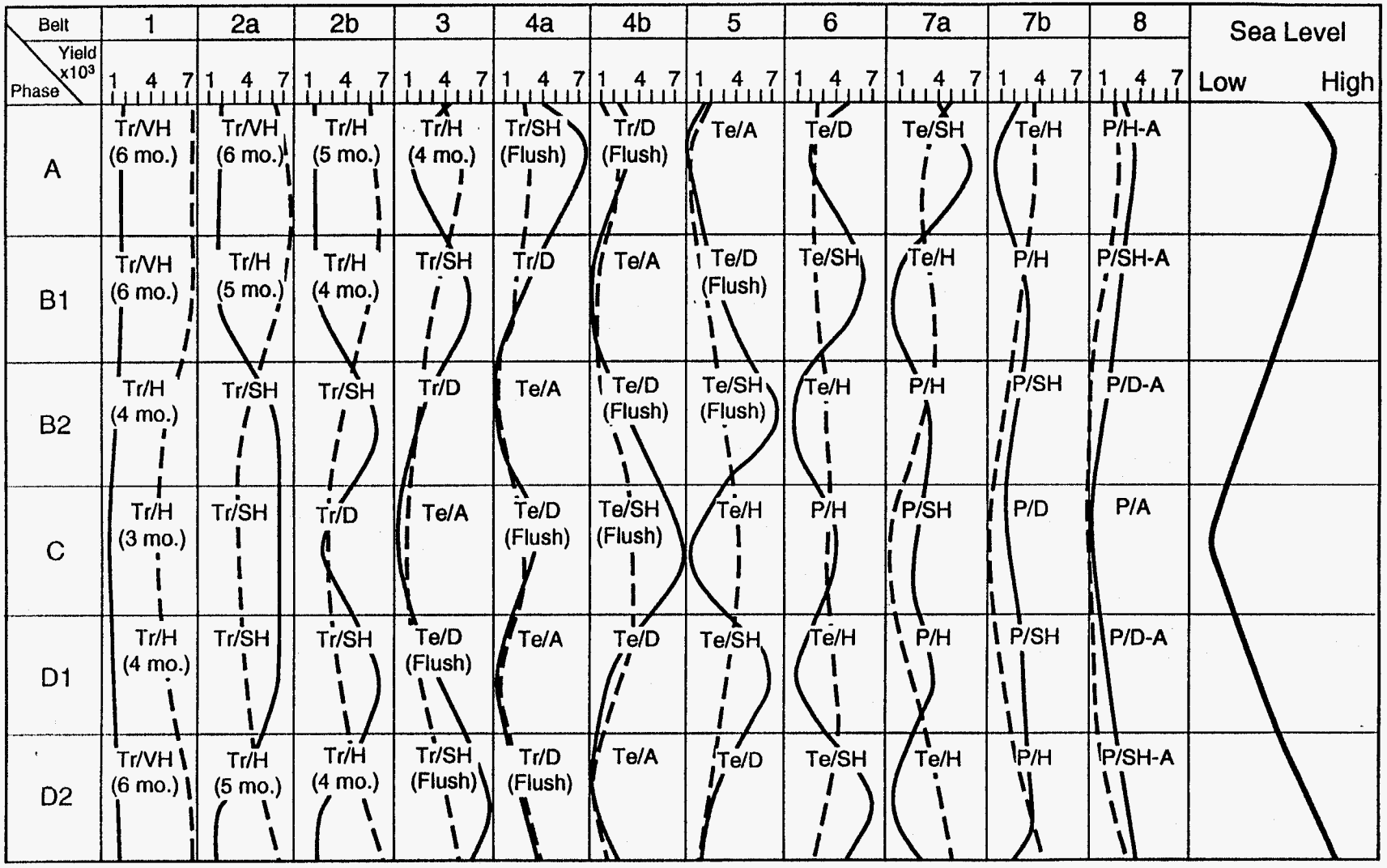

Monsoons (Kg/Km² - yr)	Temperate (Kg/Km² - yr)	Polar (Kg/Km² - yr)
6 months = 2000	Subhumid = 6500	Humid = 3500
5 months = 1700*	Dry = 2000	Subhumid = 2500*
4 months = 1400*	Humid = 200	Dry = 1500*
3 months = 1100*	Arid = 20*	Arid = 5*

*Estimated from data.

Sediment Flux
Lake Level
Sea Level

Assumptions: Tropical ≈ Temperate
Flushes add 1000.

T-8-5

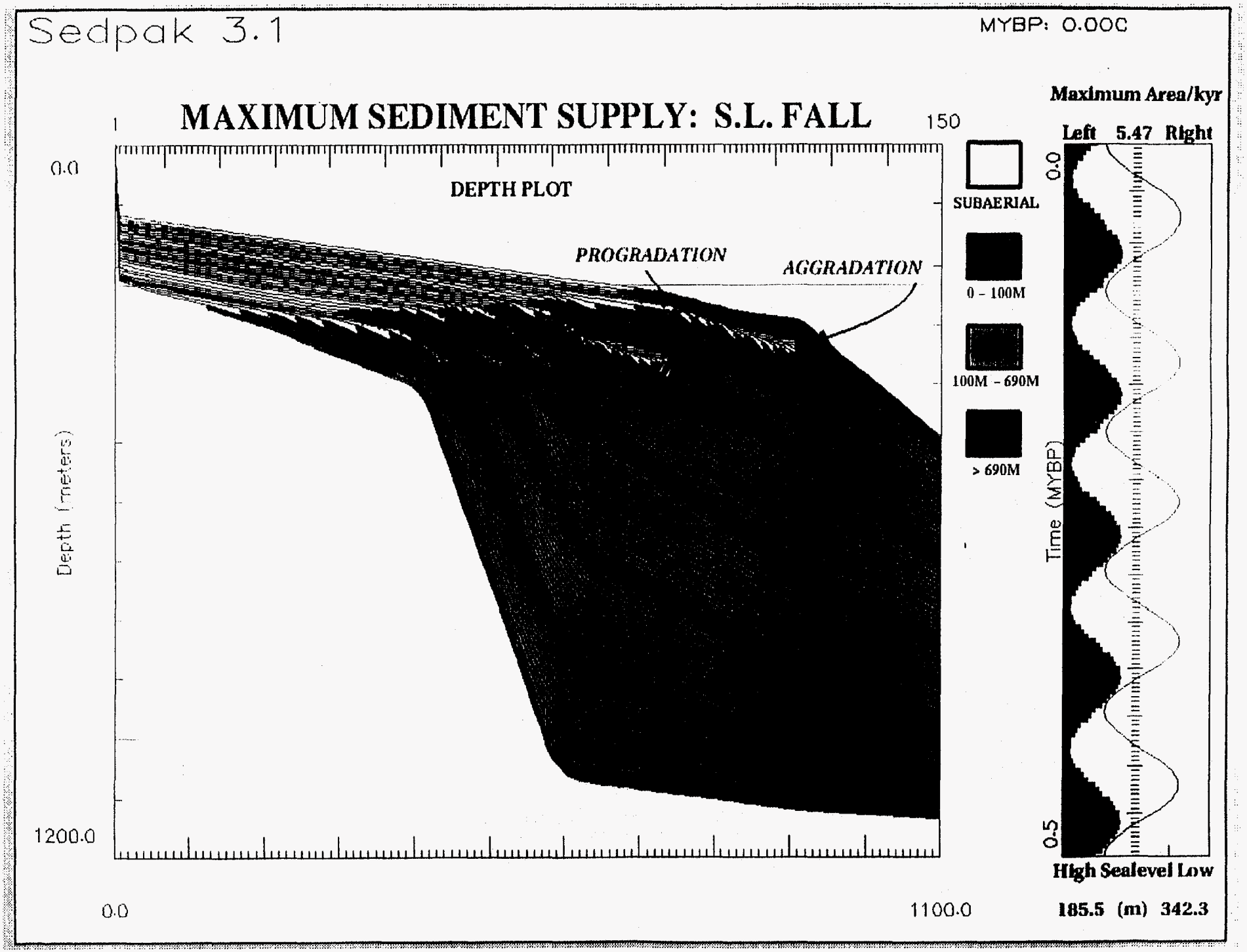
Sedpak 3.1
MYBP: 0.000
MAXIMUM SEDIMENT SUPPLY: S.L. FALL
DEPTH PLOT
PROGRADATION
AGGRADATION
SUBAERIAL
0 - 100M
100M - 690M
> 690M
Depth (meters)
0.0
1200.0
1
150
0.0
1100.0
Maximum Area/kyr
Left 5.47 Right
Time (MYBP)
0.0
0.5
High Sealevel Low
185.5 (m) 342.3

Fig. 6

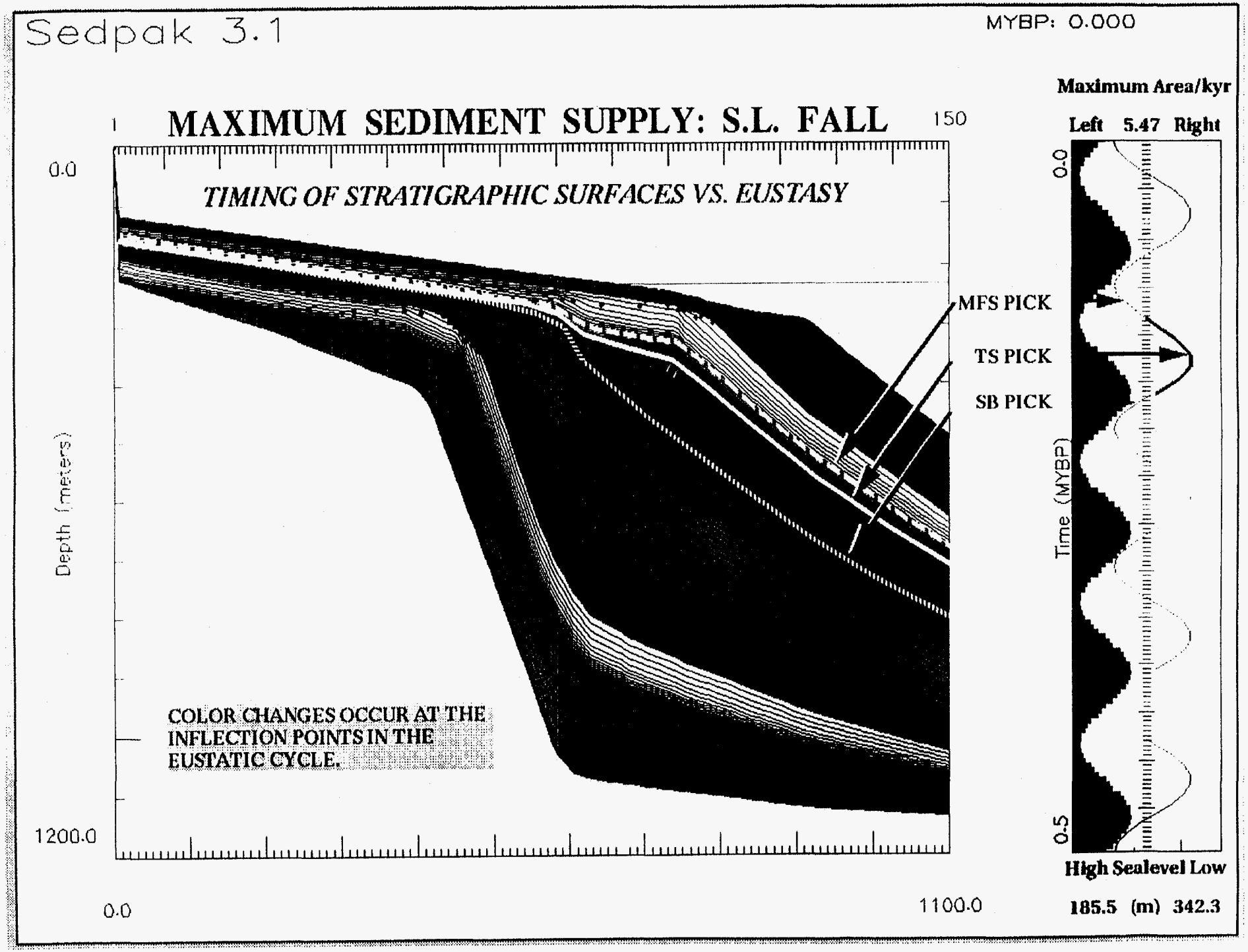
Sedpak 3.1
MYBP: 0.000
MAXIMUM SEDIMENT SUPPLY: S.L. FALL
TIMING OF STRATIGRAPHIC SURFACES VS. EUSTASY
0.0
150
1200.0
0.0
1100.0
Depth (meters)
MFS PICK
TS PICK
SB PICK
COLOR CHANGES OCCUR AT THE INFLECTION POINTS IN THE EUSTATIC CYCLE.
Maximum Area/kyr
Left 5.47 Right
0.0
0.5
Time (MYBP)
High Sealevel Low
185.5 (m) 342.3

Fig. 5

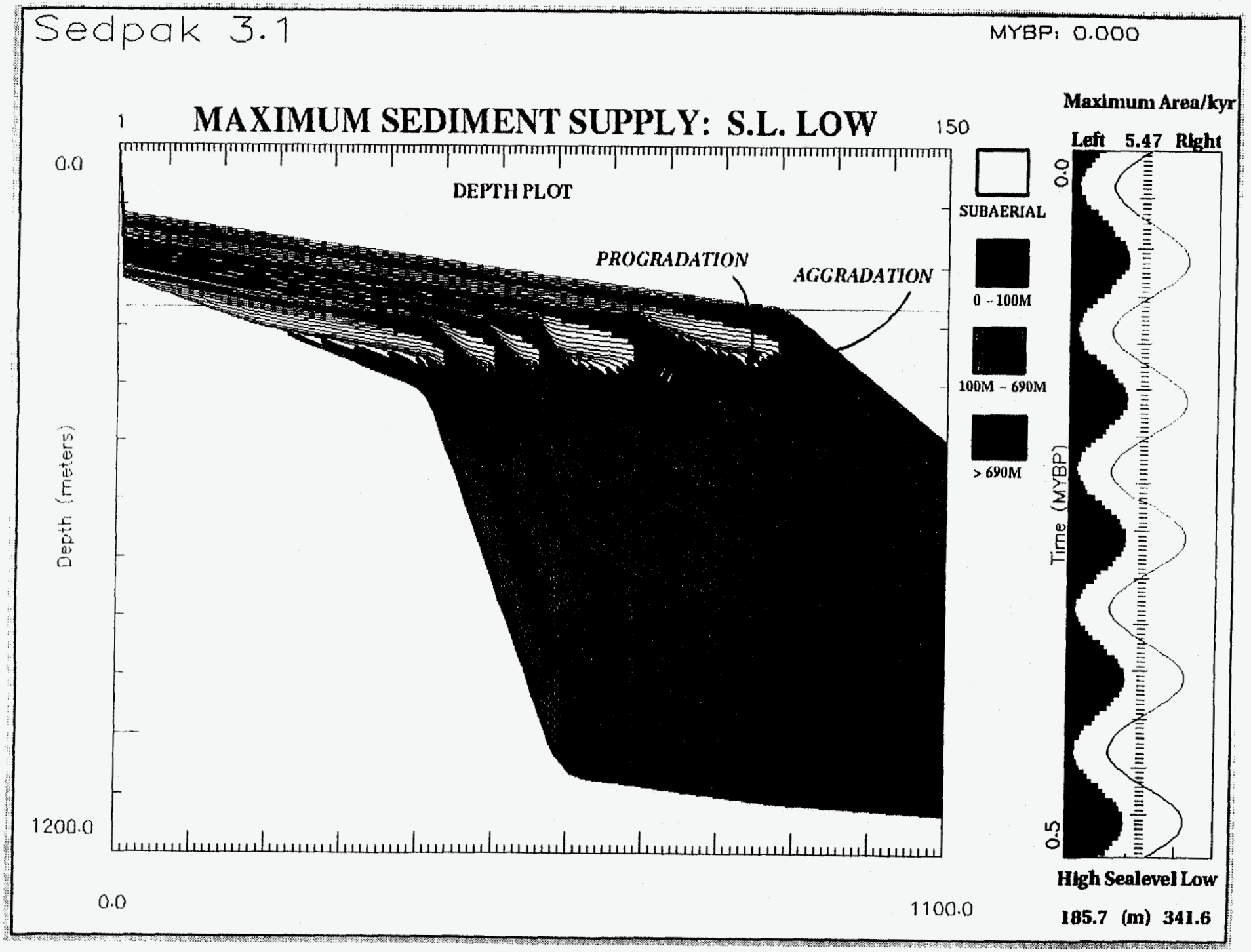
Sedpak 3.1
MYBP: 0.000
MAXIMUM SEDIMENT SUPPLY: S.L. LOW
1
150
0.0
DEPTH PLOT
PROGRADATION
AGGRADATION
SUBAERIAL
0 - 100M
100M - 690M
> 690M
Depth (meters)
1200.0
0.0
1100.0
Maximum Area/kyr
Left 5.47 Right
0.0
Time (MYBP)
0.5
High Sealevel Low
185.7 (m) 341.6

Fig. 8

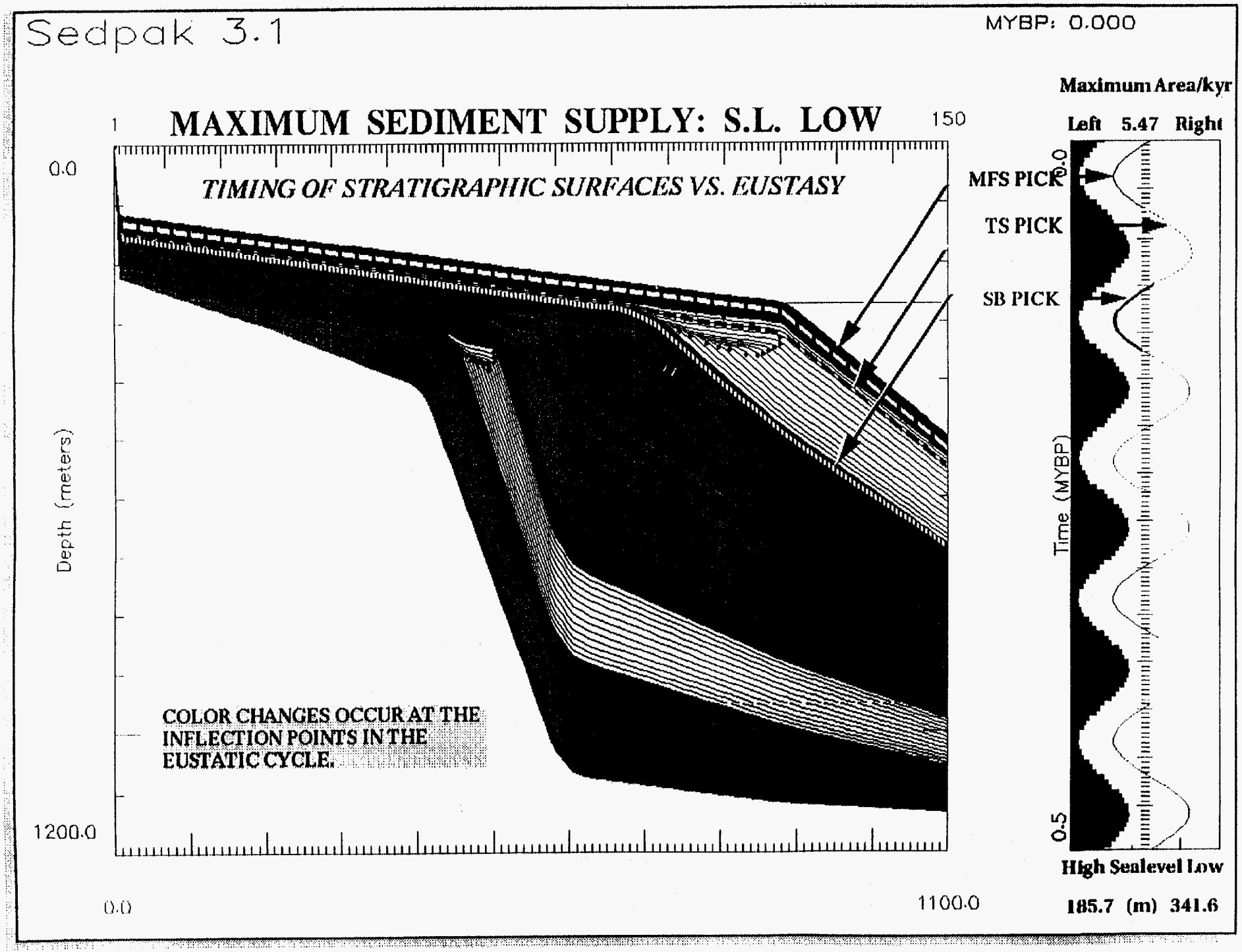
Sedpak 3.1
MYBP: 0.000
MAXIMUM SEDIMENT SUPPLY: S.L. LOW
1
150
0.0
TIMING OF STRATIGRAPHIC SURFACES VS. EUSTASY
Depth (meters)
COLOR CHANGES OCCUR AT THE INFLECTION POINTS IN THE EUSTATIC CYCLE.
1200.0
0.0
1100.0
Maximum Area/kyr
Left 5.47 Right
MFS PICK
TS PICK
SB PICK
0.0
Time (MYBP)
0.5
High Sealevel Low
185.7 (m) 341.6

Fig. 9

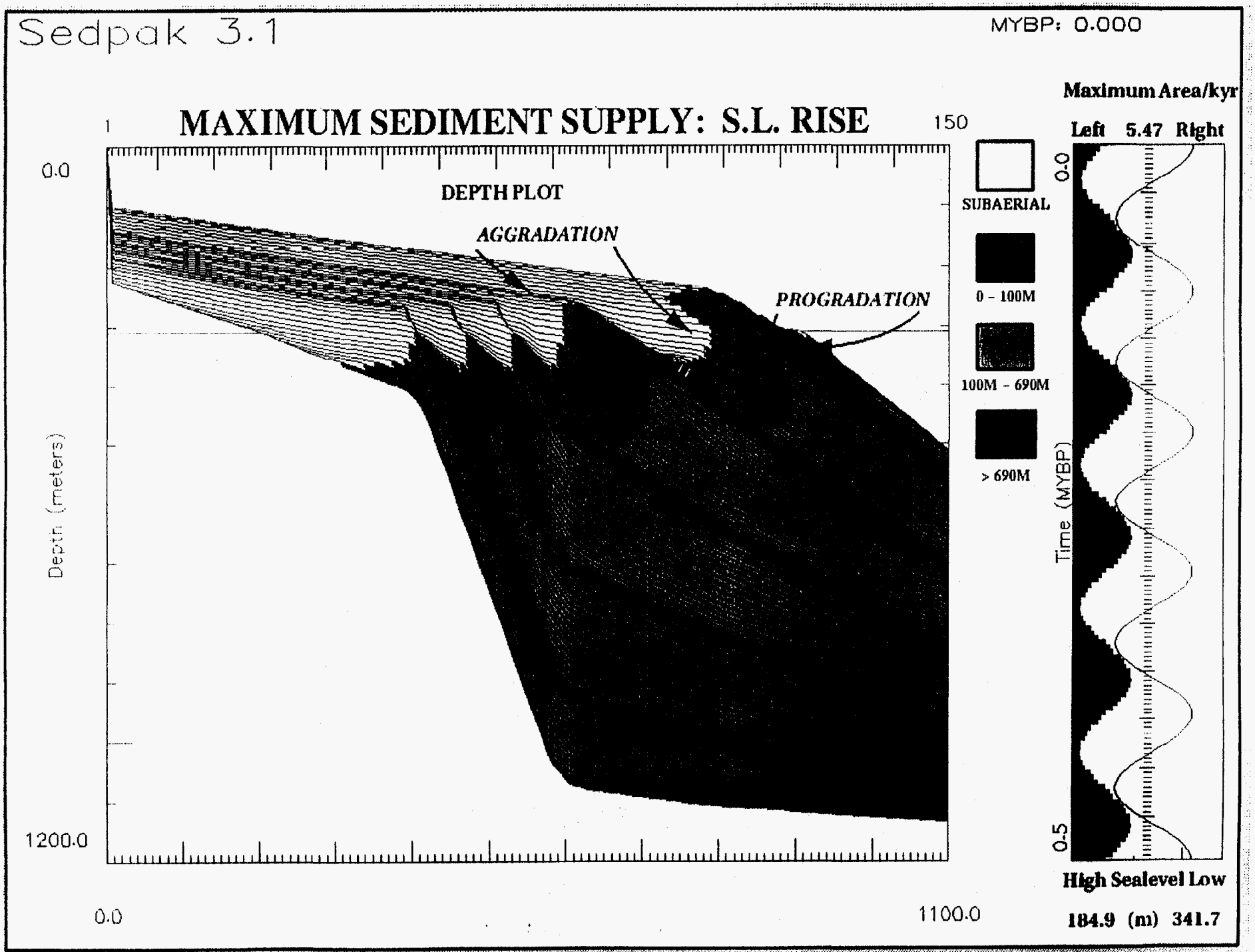
Sedpak 3.1
MYBP: 0.000
MAXIMUM SEDIMENT SUPPLY: S.L. RISE
1
150
0.0
DEPTH PLOT
AGGRADATION
PROGRADATION
Depth (meters)
1200.0
0.0
1100.0
SUBAERIAL
0 - 100M
100M - 690M
> 690M
Maximum Area/kyr
Left 5.47 Right
0.0
Time (MYBP)
0.5
High Sealevel Low
184.9 (m) 341.7

Fig. 10

Sedpak 3.1

MYBP: 0.000

MAXIMUM SEDIMENT SUPPLY: S.L. RISE

TIMING OF STRATIGRAPHIC SURFACES VS. EUSTASY

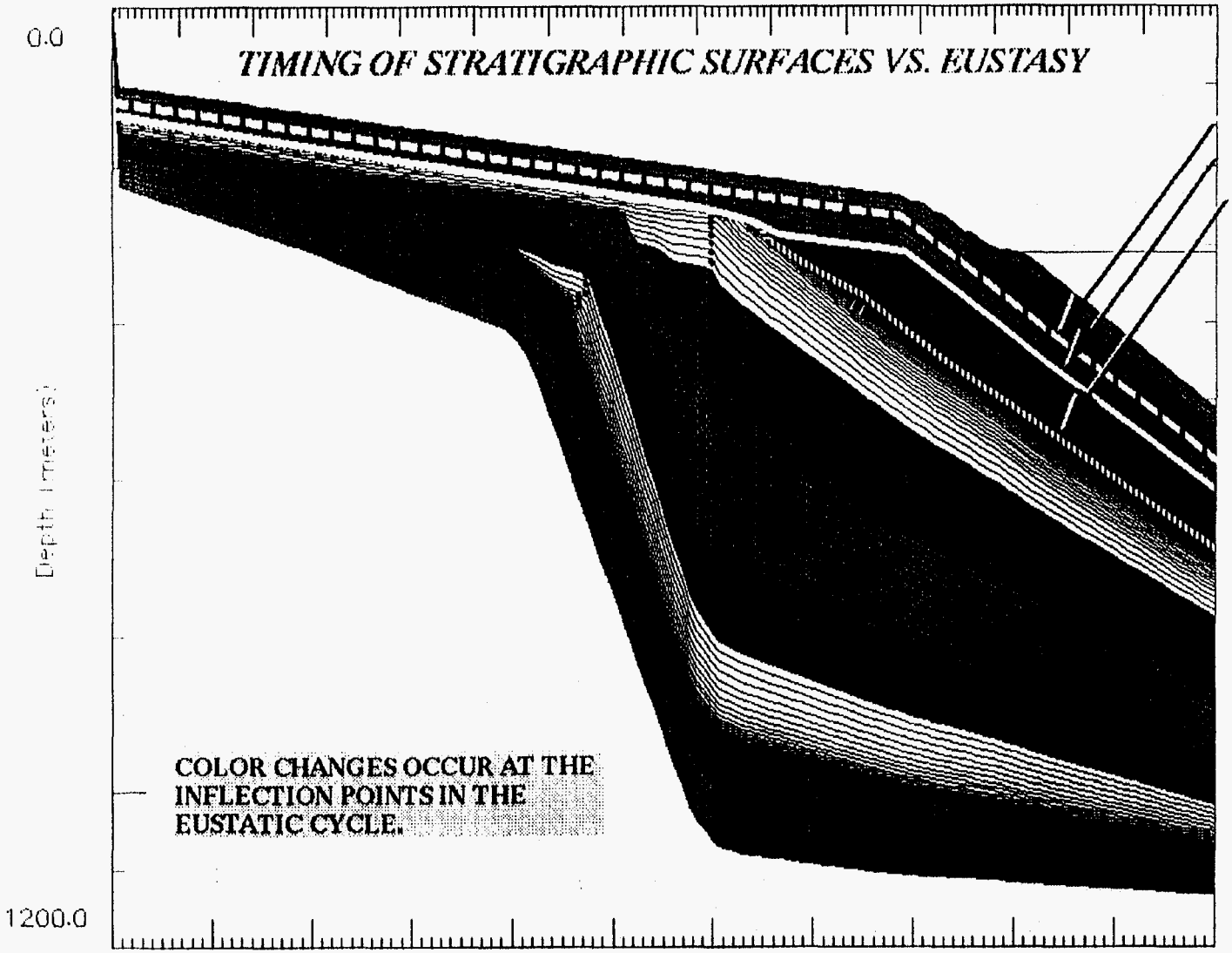

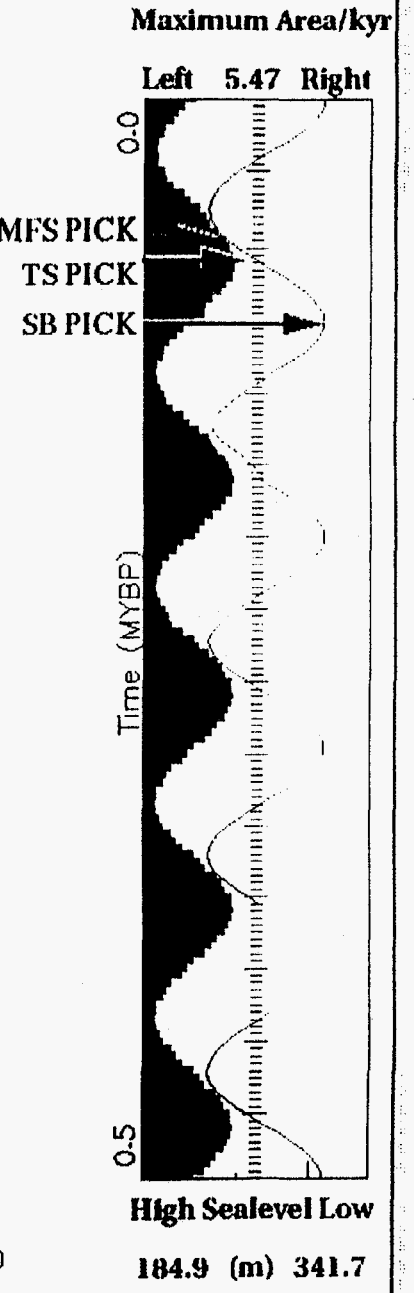

11.9.11

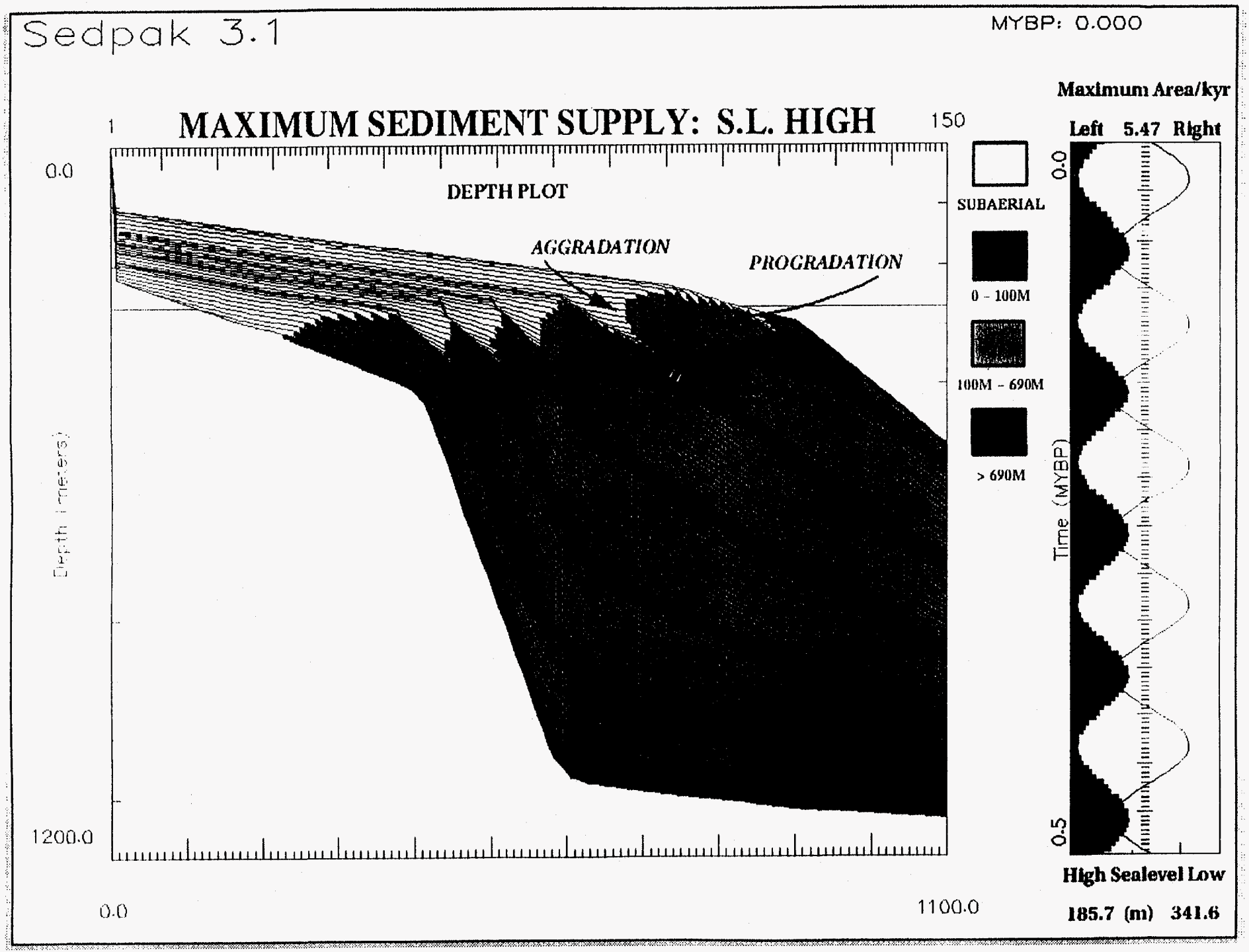
Sedpak 3.1
MYBP: 0.000
MAXIMUM SEDIMENT SUPPLY: S.L. HIGH
1
150
0.0
DEPTH PLOT
AGGRADATION
PROGRADATION
SUBAERIAL
0 - 100M
100M - 690M
> 690M
Depth (meters)
1200.0
0.0
1100.0
Maximum Area/kyr
Left 5.47 Right
0.0
Time (MYBP)
0.5
High Sealevel Low
185.7 (m) 341.6

Fig. 2

Sedpak 3.1

MYBP: 0.000

MAXIMUM SEDIMENT SUPPLY: S.L. HIGH

TIMING OF STRATIGRAPHIC SURFACES VS. EUSTASY

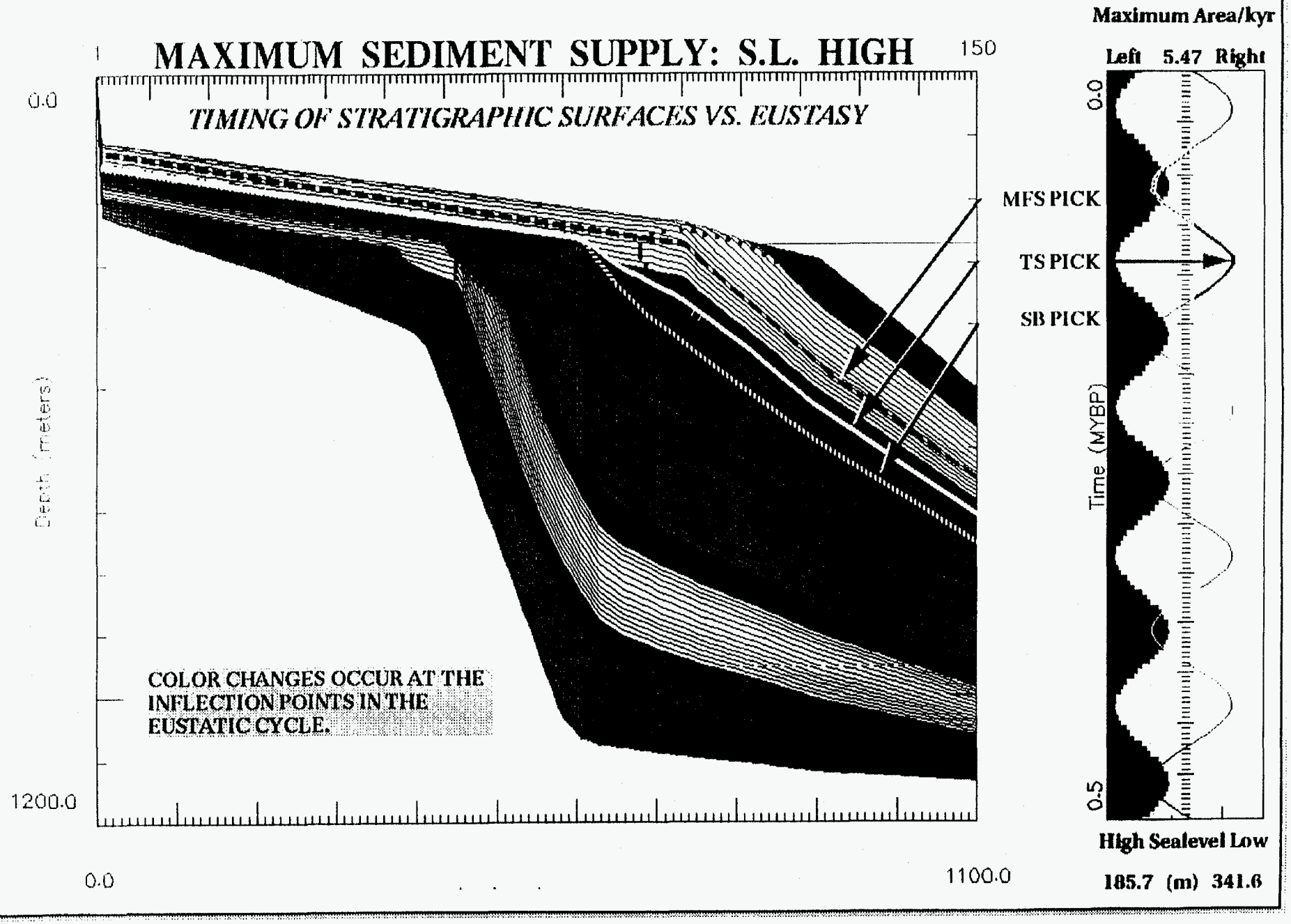

Fig. 3.1

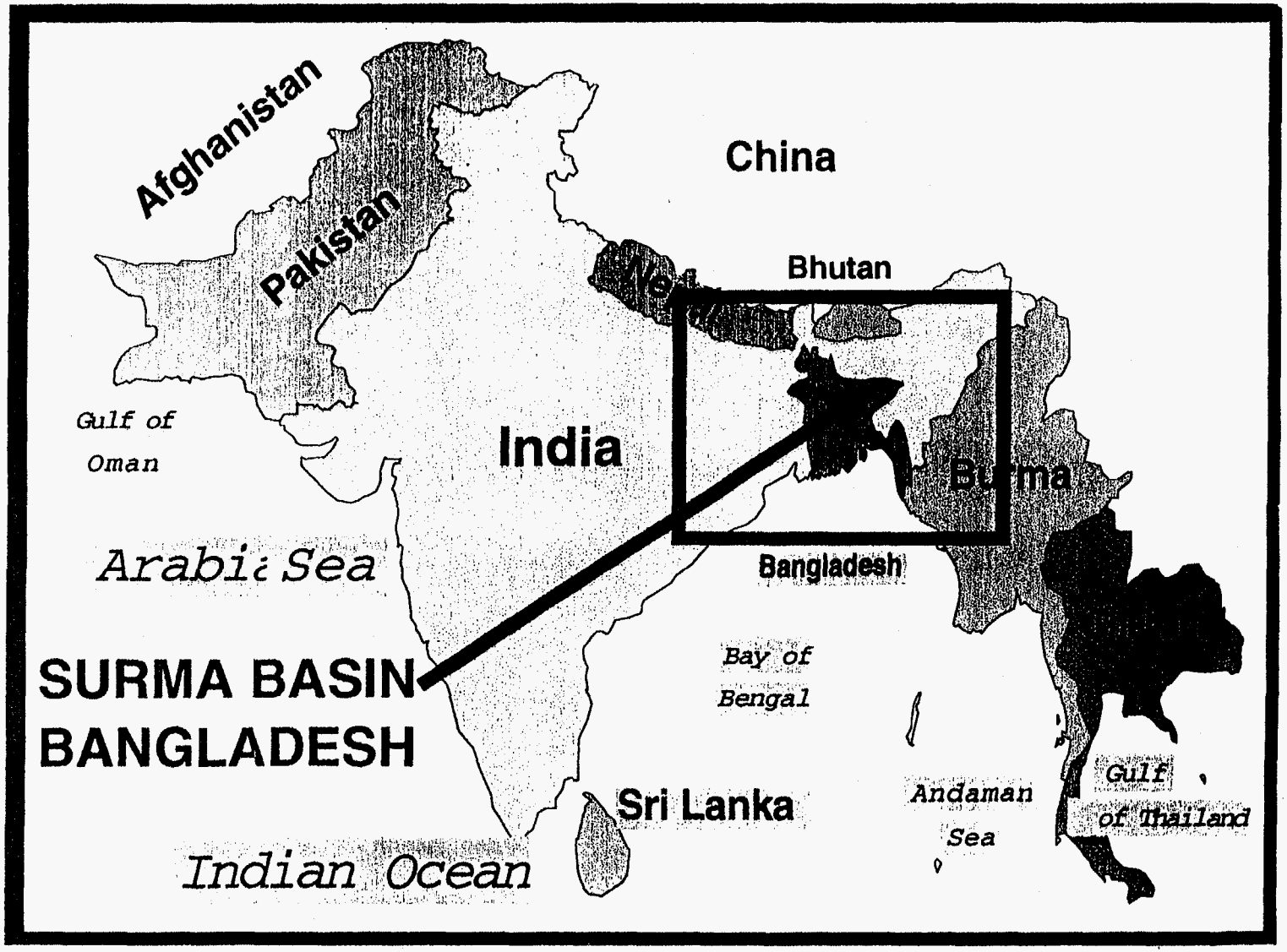
Afghanistan
Pakistan
China
Nepal
Bhutan
India
Burma
Gulf of
Oman
Arabian Sea
Bangladesh
SURMA BASIN
BANGLADESH
Bay of
Bengal
Sri Lanka
Andaman
Sea
Gulf
of Thailand
Indian Ocean

Fig. 1a

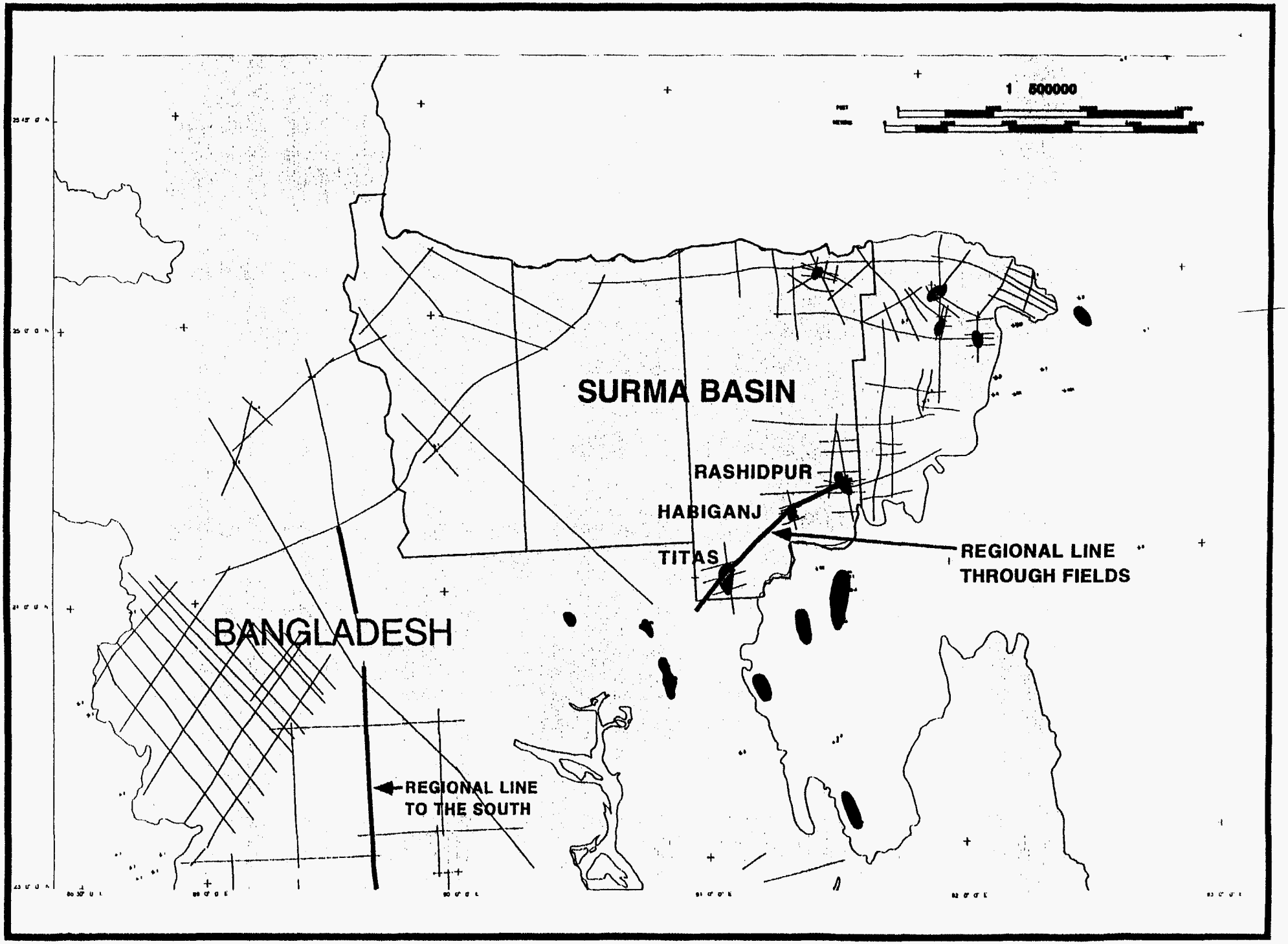
1 500000
SURMA BASIN
RASHIDPUR
HABIGANJ
TITAS
REGIONAL LINE
THROUGH FIELDS
BANGLADESH
REGIONAL LINE
TO THE SOUTH

Fig. 16

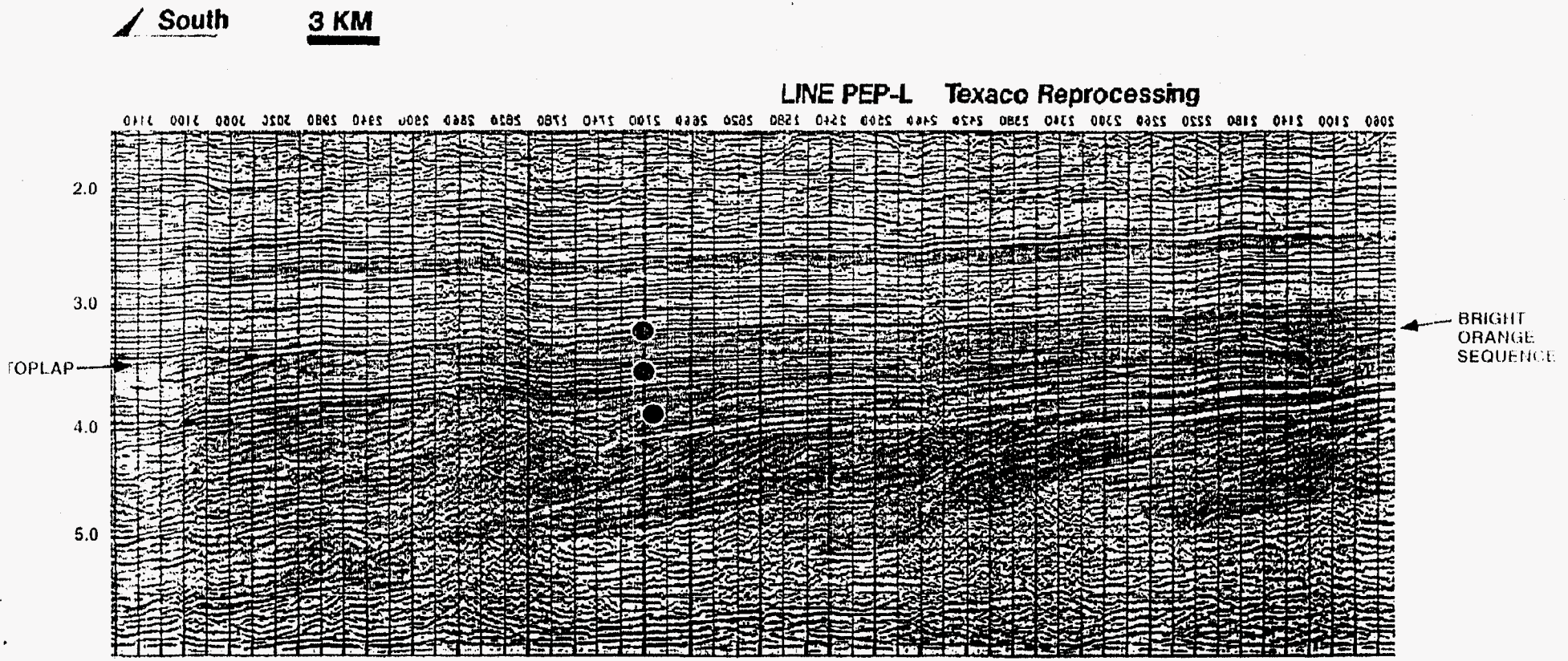
South
3 KM
LINE PEP-L Texaco Reprocessing
2.0
3.0
4.0
5.0
TOPLAP
BRIGHT
ORANGE
SEQUENCE

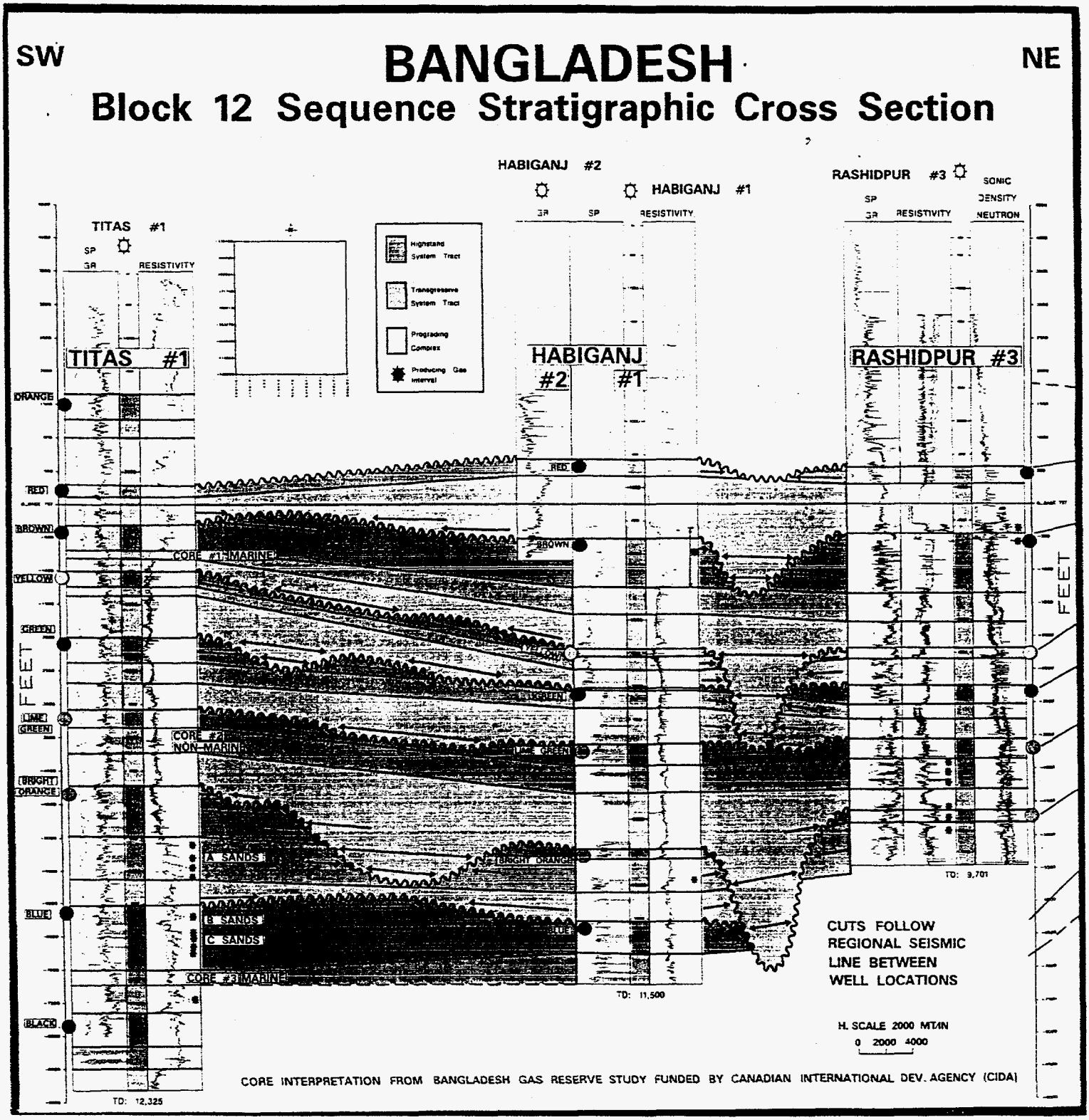
SW
BANGLADESH
NE
Block 12 Sequence Stratigraphic Cross Section
TITAS #1
SP
GR
RESISTIVITY
HABIGANJ #2
HABIGANJ #1
RASHIDPUR #3
SONIC
DENSITY
NEUTRON
Highstand System Tract
Transgressive System Tract
Prograding Complex
Producing Gas Interval
ORANGE
RED
BROWN
YELLOW
GREEN
LIME GREEN
BRIGHT ORANGE
BLUE
BLACK
CORE #1 MARINE
CORE #2 NON-MARINE
CORE #3 MARINE
A SANDS
B SANDS
C SANDS
FEET
TD: 12,325
TD: 11,500
TD: 9,701
CUTS FOLLOW REGIONAL SEISMIC LINE BETWEEN WELL LOCATIONS
H. SCALE 2000 MT/IN
0 2000 4000
CORE INTERPRETATION FROM BANGLADESH GAS RESERVE STUDY FUNDED BY CANADIAN INTERNATIONAL DEV. AGENCY (CIDA)

Fig. 16

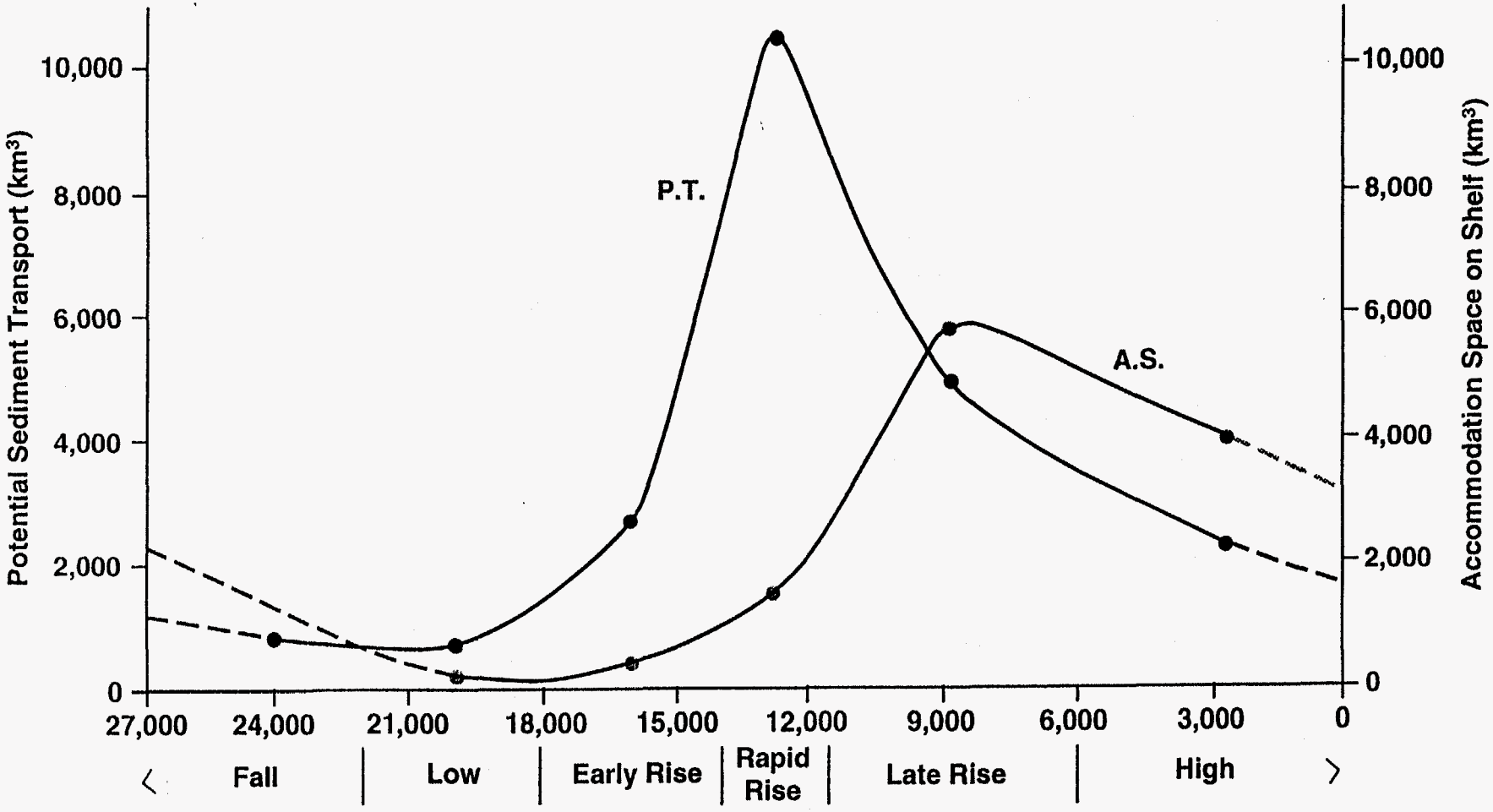
Potential Sediment Transport (km³)
Accommodation Space on Shelf (km³)
10,000
8,000
6,000
4,000
2,000
0
P.T.
A.S.
27,000
24,000
21,000
18,000
15,000
12,000
9,000
6,000
3,000
0
Fall
Low
Early Rise
Rapid Rise
Late Rise
High

Fig. 17

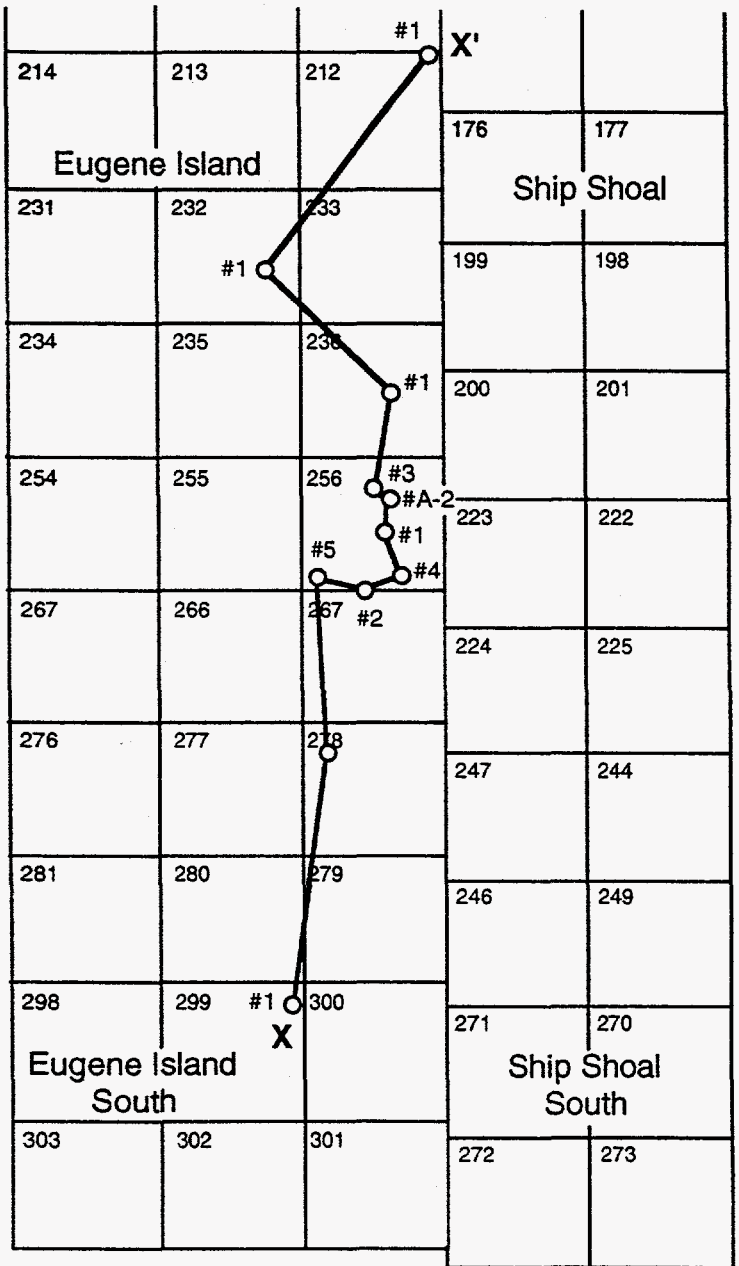

(After Radovich et al. 1990)

Fig. 18

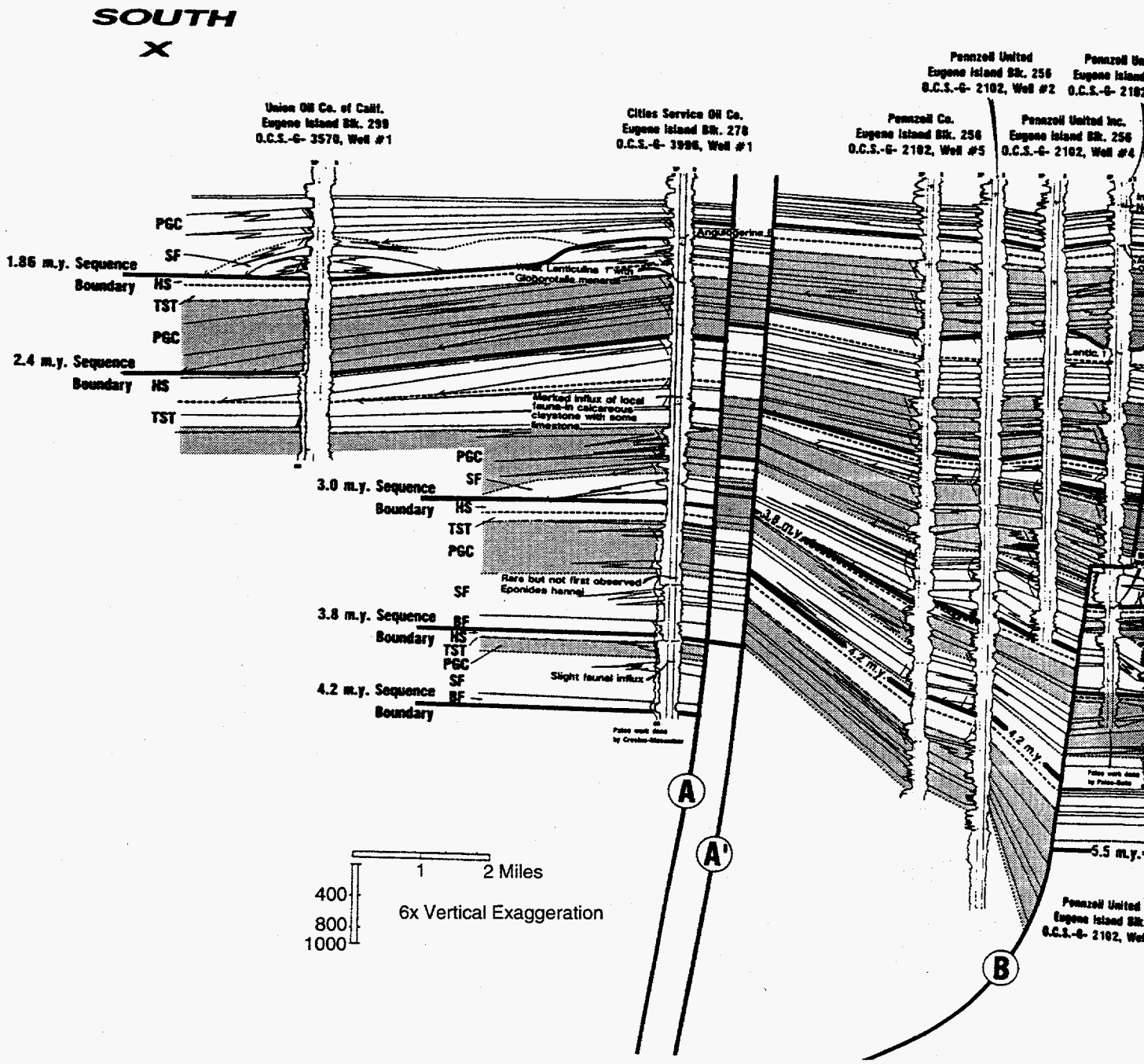
SOUTH
X
Union Oil Co. of Calif.
Eugene Island Blk. 299
O.C.S.-G- 3578, Well #1
Cities Service Oil Co.
Eugene Island Blk. 278
O.C.S.-G- 3996, Well #1
Pennzoil Co.
Eugene Island Blk. 256
O.C.S.-G- 2102, Well #5
Pennzoil United Inc.
Eugene Island Blk. 256
O.C.S.-G- 2102, Well #4
Pennzoil United
Eugene Island Blk. 256
O.C.S.-G- 2102, Well #2
PGC
SF
1.86 m.y. Sequence Boundary
HS
TST
PGC
2.4 m.y. Sequence Boundary
HS
TST
Marked influx of local fauna-in calcareous claystone with some limestone
PGC
SF
3.0 m.y. Sequence Boundary
HS
TST
PGC
SF
Rare but not first observed Eponides hannai
3.8 m.y. Sequence Boundary
BF
HS
TST
PGC
SF
Slight faunal influx
4.2 m.y. Sequence Boundary
BF
3.8 m.y.
4.2 m.y.
5.5 m.y.
A
A'
B
1
2 Miles
400
800
1000
6x Vertical Exaggeration

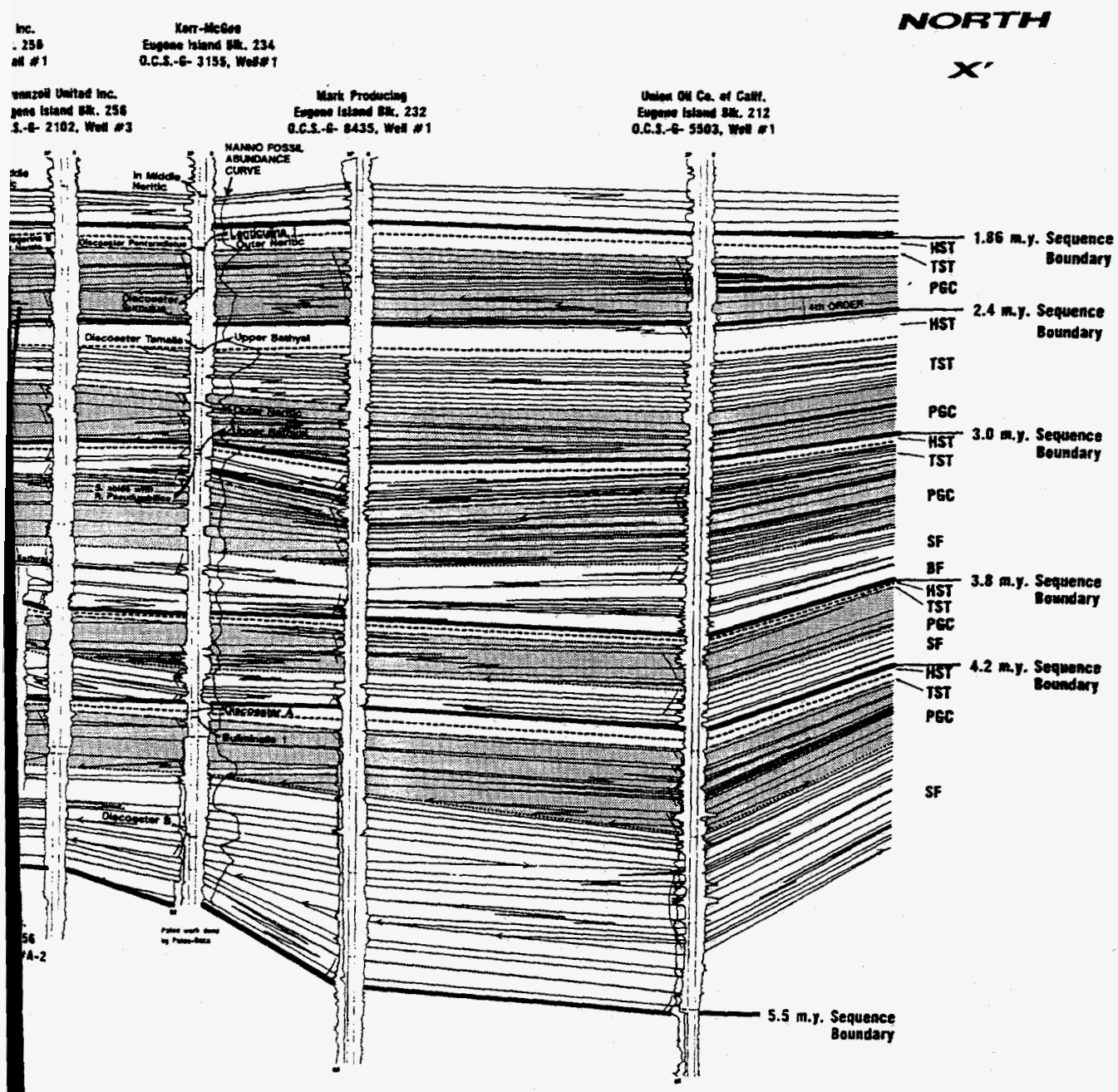
NORTH
X'
Inc.
. 258
ell #1
Kerr-McGee
Eugene Island Blk. 234
O.C.S.-G- 3155, Well#1
nzoil United Inc.
gene Island Blk. 256
S.-G- 2102, Well #3
Mark Producing
Eugene Island Blk. 232
O.C.S.-G- 8435, Well #1
Union Oil Co. of Calif.
Eugene Island Blk. 212
O.C.S.-G- 5503, Well #1
NANNO FOSSIL ABUNDANCE CURVE
In Middle Neritic
Discoaster Pentaradiatus
Discoaster Surculus
Discoaster Tamalis
Upper Bathyal
Discoaster A
Discoaster B
4th ORDER
1.86 m.y. Sequence Boundary
HST
TST
PGC
2.4 m.y. Sequence Boundary
HST
TST
PGC
3.0 m.y. Sequence Boundary
HST
TST
PGC
SF
BF
3.8 m.y. Sequence Boundary
HST
TST
PGC
SF
4.2 m.y. Sequence Boundary
HST
TST
PGC
SF
5.5 m.y. Sequence Boundary

Fig. 19

Climate Belt / Phase	Belt 1	Belt 2a	Belt 2b	Belt 3	Belt 4a	Belt 4b	Belt 5	Belt 6	Belt 7a	Belt 7b	Belt 8
Climatic Maximum Phase A	Tropical Very Humid (6 mo.)	Tropical Very Humid (6 mo.)	Tropical Humid (5 mo.)	Tropical Humid (4 mo.)	Tropical Subhumid	Tropical Dry	Temperate Arid	Temperate Dry	Temperate Subhumid	Temperate Humid	Polar Humid to Dry
Cooling Transition Phase B1	Tropical Very Humid (5 mo.)	Tropical Humid (5 mo.)	Tropical Humid (4 mo.)	Tropical Subhumid	Tropical Dry	Temperate Arid	Temperate Dry	Temperate Subhumid	Temperate Humid	Polar Humid	Polar Subhumid to Arid
Cooling Transition Phase B2	Tropical Humid (4 mo.)	Tropical Subhumid	Tropical Subhumid	Tropical Dry	Temperate Arid	Temperate Dry	Temperate Subhumid	Temperate Humid	Polar Humid	Polar Subhumid	Polar Dry to Arid
Climatic Minimum Phase C	Tropical Humid (3 mo.)	Tropical Subhumid	Tropical Dry	Temperate Arid	Temperate Dry	Temperate Subhumid	Temperate Humid	Polar Humid	Polar Subhumid	Polar Dry	Polar Arid
Warming Transition Phase D1	Tropical Humid (4 mo.)	Tropical Subhumid	Tropical Subhumid	Tropical Dry	Temperate Arid	Temperate Dry	Temperate Subhumid	Temperate Humid	Polar Humid	Polar Subhumid	Polar Dry to Arid
Warming Transition Phase D2	Tropical Very Humid (6 mo.)	Tropical Humid (5 mo.)	Tropical Humid (4 mo.)	Tropical Subhumid	Tropical Dry	Temperate Arid	Temperate Dry	Temperate Subhumid	Temperate Humid	Polar Humid	Polar Subhumid to Arid

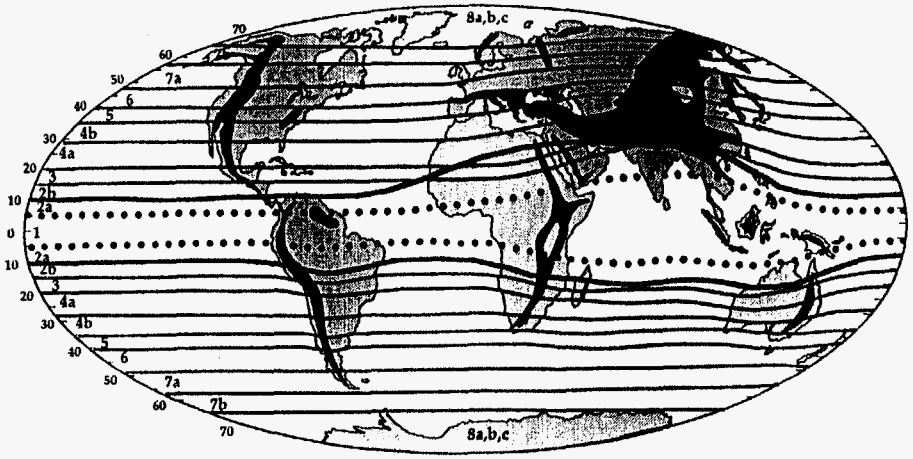

0-3 MYA

Time of Occurrence of Surfaces and Strata Relative to Eustasy

Phase Shift of Yield & Eustasy (Max. yield) / Surfaces & Strata	Sequence Boundary	Transgressive Surface	Maximum Flooding Surface	Condensed Section	Lowstand Prograding Complex
90° (Fall)	Mid Fall – just prior to the inflection point	Very Early Rise – just after lowstand	Very Late Rise – just prior to highstand	Rise	Very Late Fall and Lowstand
180° (Low)	Very Early Fall – just after highstand	Early Rise	Highstand	Highstand	Low to Early Rise
270° (Rise)	Lowstand	Mid Rise – at the inflection point	Very Late Rise – just prior to highstand	Fall	Mid Rise
360° (High)	Early Fall – midway between highstand and the inflection point	Lowstand	Late Rise – midway between the inflection point and highstand	Lowstand	Late Fall